

SYNTHESIS OF COBALT AND COBALT OXIDE FILLED CARBON NANOTUBES



A thesis submitted towards partial fulfillment of
BS-MS Dual Degree Programme

By

NITESH KUMAR SINGH

under the guidance of

Dr. ASHNA BAJPAI


RAMANUJAN FELLOW

INDIAN INSTITUTE OF SCIENCE EDUCATION AND RESEARCH
PUNE

Certificate

This is to certify that this thesis entitled “**SYNTHESIS OF COBALT AND COBALT OXIDE FILLED CARBON NANOTUBES**” submitted towards the partial fulfillment of the BS-MS dual degree programme at the Indian Institute of Science Education and Research Pune represents original research carried out by “Nitesh Kumar Singh” at “Indian Institute of Science Education and Research Pune”, under the supervision of “Dr. Ashna Bajpai” during thr academic year 2016-2017.

Nitesh Kumar Singh
Student
NAME
Nitesh Kumar Singh


Supervisor
NAME
Dr. Ashna Bajpai

Committee:
Dr. Ashna Bajpai
Dr. G. V. Pavan Kumar

Declaration

I hereby that the matter embodied in the report entitled Synthesis Of Cobalt and Cobalt Oxide Filled Carbon Nanotubes are the results of the investigation carried out by me at the Department of Physics, Indian Institute of Science Education and Research, Pune, under the supervision of Dr. Ashna Bajpai and the same has not been submitted elsewhere for any other degree.

Nitesh. Ku. Singh
Student

NAME

Nitesh Kumar Singh



Supervisor

NAME

Dr. Ashna Bajpai

Acknowledgements

I am highly indebted to express my gratitude and sincere thanks to my supervisor, Dr. Ashna Bajpai for her inspiring guidance and constant support throughout the project. I am grateful for having a wonderful opportunity to work in her lab.

I would like to express my gratitude and sincere thanks to my lab members Aakanksha Kapoor, Suvidyakumar Homkar and Namrata Patanayak for correcting my mistakes and helping me with their valuable suggestions.

I would like to thank Dr. Sunil Nair and his lab member Charu Garg for all her help with the dc magnetic measurements.

I am particularly grateful to Dr. G. V. Pawan Kumar and his lab member Rajath Sawant for helping me with the Raman measurements.

I would like to thank Dr. Shouvik Datta and his lab member Dipti and Mohit for helping me with the gold coating using sputtering method.

I would like to thank the technical staff of \hbar , Nilesh Dumbare, Anil Shetty, T. S. Yatish and Prashanth Kale for their valuable support and advises.

I would like to thank all my friends Dinesh, Gyan, Abhishek, Anand, Priyadarshi, Mayur, Brijesh and all my other batchmates for all the best and worst moment that we have had at IISER.

I would like to give special thank to Kanishk for keeping me refreshed by playing Tekken, a game which I recently explored.

Finally, I would like to thank my parents and sisters for their huge support and IISER Pune for giving me an excellent platform to do research.

Abstract

Carbon nanotubes (CNT) are one of the most fascinating discoveries in 20th century which exhibits superior properties in mechanical , electrical, optical and thermal properties. CNT can be either semiconducting or metallic, based on its chirality. Electronic industry uses CNT as an active element in the fabrication of electrical circuit. CNT can also be used for spintronics applications. Spintronics has emerged as a new field where electron spin is used as a carrier of information instead of electron charge.

Fe filled CNT are usually synthesized by pyrolysis of ferrocene, however this process is not known to yield good quality Ni and Co filled CNT. In the present work, the synthesis of cobalt-filled multi - walled carbon nanotubes has been achieved by the process of Chemical Vapor Deposition using pyrolysis of Cobaltocene. Here cobaltocene along with camphor was used as a precursor. This combination yields highly aligned forests of Co filled CNT with length of the forest upto a few 100 micro-meters. Synthesis of these filled tubes has been achieved by adjusting experimental parameters like sublimation temperature, pyrolysis temperature, argon flow rate and the amount of precursor. These samples have been characterized by Raman, X-ray diffraction and Scanning Electron Microscopy. The Raman spectroscopy shows well defined D and G bands with the I_d/I_g ratio of 0.639 with the occurrence of 2D band as well. Magnetic measurement shows that it exhibit ferromagnetic behaviour with the coercive field of 660 Oe due the filling of cobalt inside the nanotube shell. These filled CNTs forests have been drop-cast on a glass substrate and preliminary electron transport measurements have also been reported here.

The aligned forest of Co filled CNT have also been converted to Co oxides by suitable annealing and the sample thus formed has been characterized by SEM, XRD and Raman. These samples are relevant for battery material as well as for spintronic applications.

Contents

1. Introduction	
1.1. History.....	8
1.2. Structure.....	9
1.2.1. Single walled nanotubes.....	9
1.2.2. Multi walled nanotubes.....	11
1.3. Properties.....	12
1.3.1. Mechanical properties.....	12
1.3.2. Electron transport properties.....	13
1.4. Application.....	15
1.4.1. Magnetic recording devices.....	15
1.4.2. Device fabrication.....	16
1.4.3. Energy storage applications.....	17
1.4.4. Spintronics applications.....	17
1.4.5. Encapsulation of magnetic oxides inside CNTs.....	17
1.5. Plan of thesis.....	18
2. Methods.....	19
2.1. Sample preparation.....	19
2.2. Characterization technique.....	19
2.2.1. Field emission scanning electron microscope.....	19
2.2.2. Powder x-ray diffraction.....	20
2.2.3. Raman spectroscopy.....	21
2.2.4. Superconducting quantum interference device.....	22
3. Cobalt filled@CNTs.....	24
3.1. Schematic of the CVD set up.....	24
3.2. Use of Camphor with Cobaltocene.....	25
3.3. SEM images.....	27
3.4. Powder x-ray diffraction.....	31
3.5. Raman spectroscopy.....	33

3.6. Magnetic measurements.....	34
3.7. Electron transport measurements.....	35
4. Conversion of aligned forest of Co@CNT to CoO _x	37
4.1. Oxidation of Co@CNT.....	37
4.2. SEM images.....	38
4.3. Powder x-ray diffraction.....	42
4.4. Raman spectroscopy.....	43
5. Summary and future work.....	44
5.1. Summary.....	44
5.2. Future plans.....	45
References.....	46

Chapter 1

Introduction

1.1. History

Carbon nanotubes (CNTs) is one of the great discoveries in the late 20th century by S. Iijima [1]. CNTs can be considered as fourth allotropes of carbon after diamond, graphite and fullerenes. CNTs have attracted many researchers all over the world due to its unusual properties and it is very promising material in the semiconductor electronics based on nanotechnology.

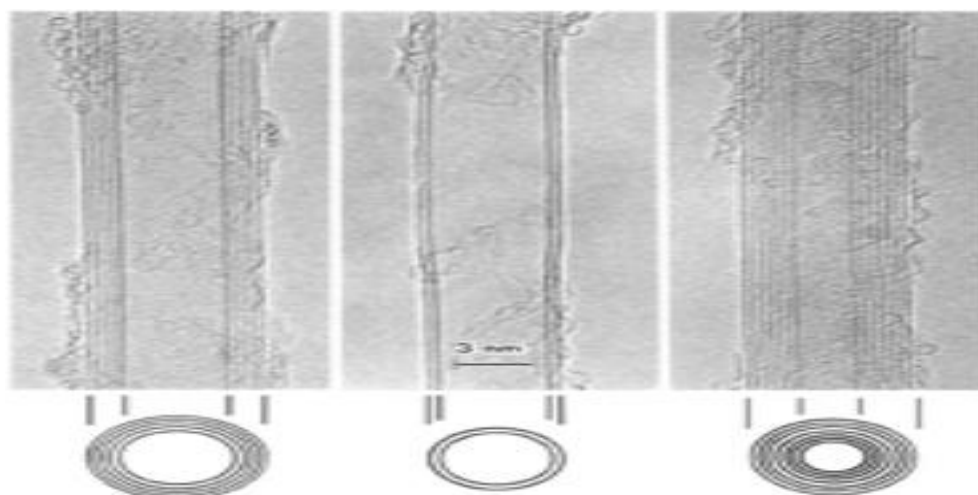


Fig 1.1 [1]: High resolution transmission electron microscope image of double and multi-wall CNTs observed by S. Iijima.

CNTs can be modified to have desired properties by controlling the growth parameters. CNTs are sheet of carbon atoms arranged in a honeycomb network with cylindrical nanostructure. These cylindrical structure of carbon atoms have never been found in nature, thus CNTs are artificially created tube like structure. These structure have very high length-to-diameter ratio up to 132,000,000:1 [2]. After the discovery of carbon nanotubes, other inorganic nanotubes have also been synthesized whose morphology is similar to carbon nanotubes [3].

1.2. Structure

The structure of CNTs can be imagined by rolling one or many single sheets of graphene in the form of 1-dimensional cylinder. The reason for many allotropes of carbon is that the valence electron of carbon atom allowing different types of orbital hybridization. Table 1.1 shows possible carbon isomers and their comparison based on different physical parameters.

Dimension	0-D	1-D	2-D	3-D
isomer	C ₆₀ fullerene	nanotube carbyne	graphite fiber	diamond amorphous
hybridization	sp^2	sp^2 (sp)	sp^2	sp^3
density [g/cm ³]	1.72	1.2-2.0 2.68-3.13	2.26 ~ 2	3.515 2-3
Bond Length [Å]	1.40(C=C) 1.46(C-C)	1.44(C=C)	1.42(C=C) 1.44(C=C)	1.54(C-C)
electronic properties	semiconductor $E_g = 1.9\text{eV}$	metal or semiconductor	semimetal	insulating $E_g = 5.47\text{eV}$

Table 1.1 [4]: Comparison of different parameter of isomer of carbon.

The arrangement of carbon atoms within the graphitic shell determine the different properties of CNTs. For example, the chirality of the CNTs determines its metallic or semiconducting behavior. The chirality of CNTs can be controlled by its growth conditions [5]. The mechanical properties of CNTs are largely depending on the carbon atoms arrangement on the graphitic shell. The presence of defects can lower the mechanical properties of CNTs. CNTs are categorized as single-walled nanotubes(SWNTs) and multi-walled nanotubes(MWNTs) depending on the number of graphitic shells. Both types of CNTs are considered important and have wide application in various fields.

1.2.1. Single Walled Nanotubes

SWNTs consist of only one graphitic shell rolled up in the form of cylinder. The diameter typically varies from 0.5nm to 3nm and it can be a few tens of cm in length [6].SWNTs are more promising as compared to MWNTs for electrical application. These one-dimensional structure can be metallic or semiconducting based upon its chirality. The chirality of nanotubes is defined by its chiral vector denoted as C_h in figure 1.2.

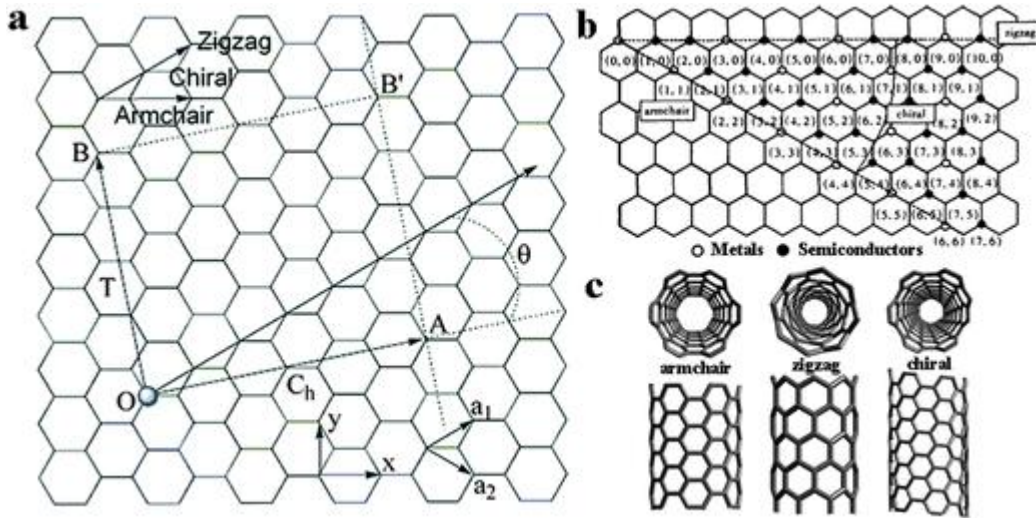


Fig 1.2 [7]: (a) Schematic of chiral vector(C_h) in 2-D graphene layer. (b) Relationship between integers (n,m) and metallic or semiconducting behavior of nanotubes. (c) The different structure on nanotubes based on chirality .

The chiral vector determine the position of any hexagon in the graphitic layer. In the Figure 1.2, OB is translation vector and OA is chiral vector in which nanotube rolls up and C_h can be written as

$$C_h = n \cdot a_1 + m \cdot a_2 \quad (1.1)$$

where n, m are integers and a_1, a_2 are basis unit vectors as shown in the hexagonal graphene layer in Figure 1.2. An angle between the chiral vector and one of the basis vector is defined as chiral angle [4]. The chiral angle θ , can also be used to denote the folding of graphene layer in the cylindrical form and its values are in between 0° and 30° . These values of θ are enough to distinctively define different types of nanotubes namely armchair, zigzag and helical CNTs. The armchair CNTs are formed for an angle $\theta = 30^\circ$ and tube coordinates (n,m) equal to (n,n) or (m,m) . The zigzag CNTs are formed for an angle $\theta = 0^\circ$ and tube coordinates equal to $(0,m)$ or $(n,0)$. A carbon nanotubes whose mirror image is exactly same as original one is defined as achiral nanotubes. The armchair and zigzag nanotubes are the two types which falls under symmetry classification as being achiral nanotubes. A carbon nanotubes whose mirror image is non-superimposable to the original one is defined as chiral nanotubes. Any other angle in between 0° and 30° leads to formation of chiral CNTs(helical) and these tubes falls under symmetry classification as being chiral nanotubes. SWNTs are

metallic when $|n - m| = 3j$, where j is an integer and if $|n - m| \neq 3j$ then nanotubes are semiconducting in nature [8]. It is very difficult to synthesize uniform metallic or semiconducting behavior throughout the bulk sample.

The diameter of SWNTs can be calculated using the chiral length (n,m) of chiral vector C_h . Diameter of nanotube can be written as:

$$D = \frac{C_h}{\pi} = \frac{a_{cc}\sqrt{3(n^2 + m^2 + nm)}}{\pi} \quad (1.2)$$

Where a_{cc} is the average carbon-carbon bond length ($1.41\text{\AA} \leq a_{cc} \leq 1.44\text{\AA}$) found in graphite [9].

The chiral angle, θ , is given by [10]:

$$\theta = \sin^{-1}\left(\frac{\sqrt{3}m}{2\sqrt{n^2 + m^2 + nm}}\right) \quad (1.3)$$

where n, m are integers.

The energy gap between the valence and conduction band of semiconducting SWNTs is given by [4]:

$$E_g = \frac{|t|a_{c-c}}{d_t} \quad (1.4)$$

where a_{c-c} is the distance between two neighboring carbon atom in the crystal lattice, d_t is the diameter of the CNT and $|t|$ is overlap integral which comes from tight-binding theory. This is quite amazing that mechanical and electrical properties of SWNTs originate from 2-D graphene whose energy gap falls under the category of semimetal.

1.2.2. Multi Walled Nanotubes

Multi walled nanotubes can be imagined as concentric SWNTs with gradual increase in diameter [1]. The perfection in arrangement of graphitic planes determines the material properties of MWNTs. The properties on MWNTs is quite different from SWNTs due to the variation of length and diameter of these structures [11]. The distance between two interlayer graphitic shell is close to 0.32 - 0.35nm [12]. The bonding between two neighboring carbon atoms in the intra-graphitic layer of CNTs is comprised of sp^2 bonds which provide them unique mechanical strength. The inter-graphitic layer of CNTs is held together by van der Waals forces.

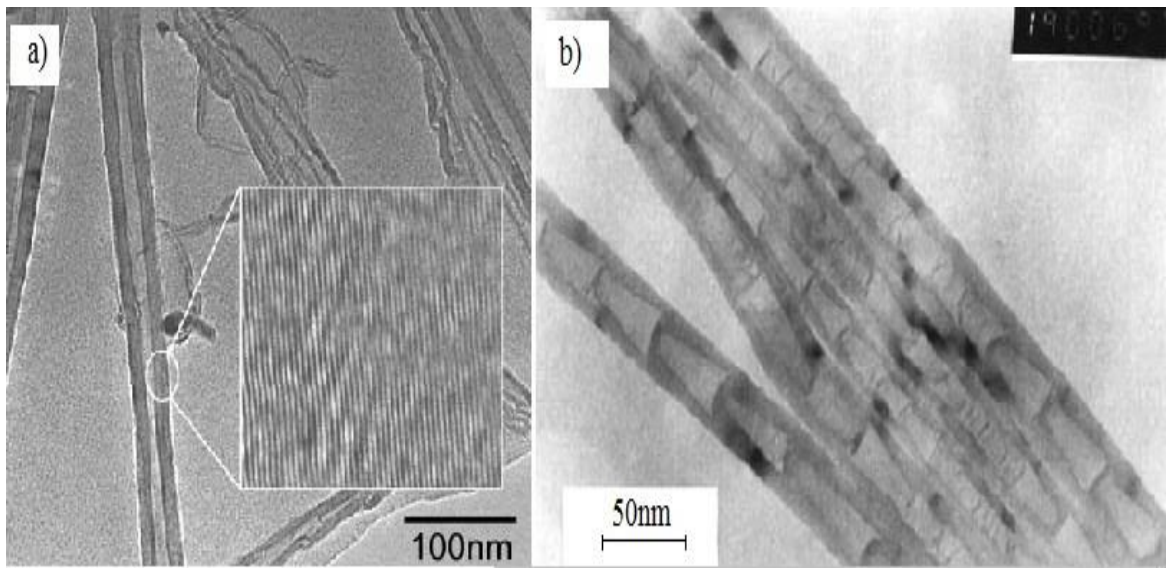


Fig 1.3 : (a) MWNTs with inset showing high degree of graphitization [13]. (b) formation of bamboo-type nanotubes due to presence of slight imperfection [14].

In the above image of different types of MWNTs, image (a) is catalytic synthesis of CNT (b) shows bamboo shaped carbon filaments.

1.3. Properties

Carbon nanotubes are 1-D structure with highly unusual properties. Its experimental and theoretical results are quite close to each other. Theoretical studies have shown that its unusual properties are due to the arrangements of carbon atoms in the form of honey-comb lattice. There can be slight variation in mechanical properties due to the presence of defects [15].

1.3.1. Mechanical Properties

CNTs have different properties in axial and radial direction based on its geometry [16]. These nanotubes are the strongest material in nature. Their strength comes from sp^2 bonding between the carbon atoms within the graphitic layer. Previous studies calculated the values of Young's modulus on the order of 270-950 GPa and tensile strength on the order of 11-63 GPa [17]. There are lots of method to measure the mechanical strength of CNTs which includes resonance measurement, microsystems tooling measurement and bulk material analysis. CNTs are excellent choice for composite filling material because of its low density and high tensile strength [18].

There was an evidence regarding the softness of CNTs in the radial direction. The first observation of radial elasticity using transmission electron microscope(TEM) showed that two adjacent nanotubes can be deformed even by weak forces like van der waals forces [19]. The knowledge of internal diameter of the CNTs is important for determination of radial elasticity and its also possible to have different internal diameter of CNTs with identical outer diameter. A new method has been introduced by researchers to determine the exact number of layers using atomic force microscopy(AFM) [20].

1.3.2. Electron Transport Properties

Electron transport measurement are carried out by passing a direct or alternating current through a source and drain electrodes. In between the source and drain electrodes, CNTs are dropcasted on the non conducting surface like SiO₂. A gate electrode can be used to vary the charge density of CNTs. By applying any constant voltage(above threshold voltage) to the gate electrode, one can apply bias across the source and drain electrodes and measure resulting currents. Fig 1.4 shows common configuration of field-effect transistor(FET) setup and used to measure the transport properties of CNTs.

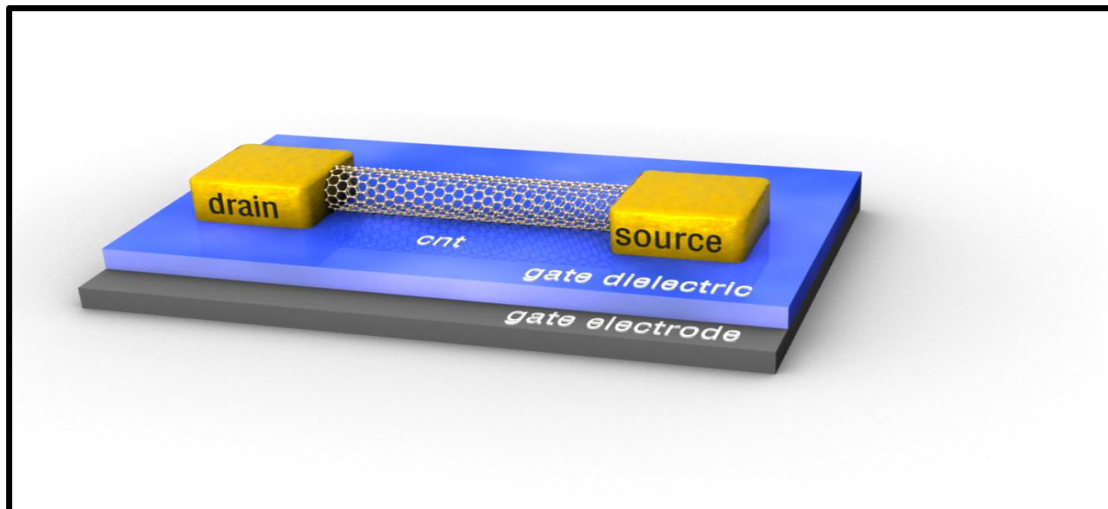


Fig 1.4 [21]: Schematic of common FET setup to measure transport properties in CNTs.

As mentioned previously, CNTs can be either metallic or semiconducting based on their chirality. It has been shown that only armchair CNTs have zero value band gap while non-armchair metallic CNTs have very small band gap due to curved geometry of CNTs which creates a small gap in its band structure [4]. The semiconducting CNTs have a band gap on the order of 0.5 to 0.8 meV in size [22].

Previous studies found that electron transport in SWNTs can result in classical or quantum transport regime because of 1-D nature of CNTs which brings the quantization of wave function of moving electrons within the circumferential graphitic lattice of CNTs [4]. The Landauer formula for conductance valid for 1-D quasi system can be written as [4]:

$$G(E) = \left(\frac{2e^2}{h}\right)M(E)T(E) \quad (1.5)$$

where $T(E)$ is the probability of transmission of electron at the Fermi level and $M(E)$ is the total number of conduction channel, for metallic CNTs $M(E)$ is 2. So it can be seen that there is a perfect transmission of electrons through the CNTs results in ballistic conduction in which there is voltage drop while going from 3-D to 1-D conductor [4]. The final conductance value, $G_q = \frac{4e^2}{h}$ is called quantum conductance

of CNTs. In the final equation, the factor of 4 comes because electron sees two 1-D sub-bands near Fermi energy when it jumps from electrode to CNT due to degeneracy of orbital [22]. The quantum conductance, G_q , converted into quantum resistance as

$R_q = \frac{1}{G_q} = 6.5K\Omega$. One must make device perfectly clean with ohmic contacts in order to reach electrical resistance close to 6.5 K Ω .

Now if the transmission probability is non-unity, then one can see diffusion regime of electron transport where voltage drop occurs not only at the contacts but it also occurs throughout the whole length of CNT. The equation for conductance will be same as Equation 1.5, but resistance will be calculated as [22]:

$$R = \frac{1}{G} = \left(\frac{h}{4e^2}\right)\left(\frac{1}{T}\right) = \left(\frac{h}{4e^2}\right) + \left(\frac{h}{4e^2}\right)\left(\frac{L}{l_m}\right) + R_{contact} \quad (1.6)$$

where L is length of CNT and l_m is mean free path which tells the average distance traveled by electron before scattering.

The mean free path in metallic CNTs has been calculated as high as 10 μm at low temperature and in case of semiconducting CNTs it is on the order of 1 μm . The diffusive regime is also called as classical transport regime with the assumption of $L \gg l_m$ which is opposite to the ballistic regime where $l_m \gg L$. As it is clear from Equation 1.6, first term is the quantum resistance of CNT and the second term is associated to the scattering of electrons moving through the CNT whereas the third

term is contact resistance. The scattering of electrons is usually caused by thermal lattice vibration called phonons.

Metallic CNTs can carry an electric current density close to 4×10^9 A/cm² and this value is 1000 times greater as compared to metals like copper [23].

Physical Property	SWNT	MWNT
Tensile Strength (GPa)	50-200 [24] 3.6-22.2 [25]	11-63 [26] 6.2-22.2 [27]
Young's Modulus (GPa)	1000 [24]	270-950 [26] 690-1870 [27]
Current Density (A/cm ²)	10^7 - 10^8 [28]	10^9 [29]
Electrical Conductivity (S/m)	1×10^6 [30]	2×10^5 [31]

Table 1.2 : Comparison of physical properties of SWNTs and MWNTs.

1.4. Applications

1.4.1. Magnetic Recording Devices

Ferromagnetic nanowires in the aligned form found application in high density magnetic recording media [32]. Due to the unique magnetic properties in nano scale dimension, these wires exhibit larger magnetic anisotropy with enhanced coercivity. But due to the higher chance of oxidation of bare metal nanowires which restricts its use in media recording applications. Recent studies have shown the encapsulation of these bare metal nanowires within CNTs which provide stability of nanowires against oxidation. Researchers have filled CNTs with ferromagnets like Fe, Co, Ni or their alloys and found these system particularly interesting due to their unique magnetic properties [33-38]. Cobalt oxide (CoO) has been used for the preservation of magnetization of small ferromagnetic nanoparticles against thermal fluctuation in Co-CoO core/shell structure which can increase the data storage in magnetic recording [39].

1.4.2. Device Fabrication

Because of superior electrical, mechanical and several other interesting properties, CNTs have been used as building blocks of nano-electronics [40]. Several studies have been carried out in the literature for the dropcasting of CNTs at the preferred location [41]. Gao et al. [42] has tried to carefully put the individual nanotubes between metal electrodes and a four-point arrangement has been realised using atomic force microscopy (AFM) manipulation. Researchers have used polydimethylsiloxane (PDMS) microchannel and directed SWNTs into these microchannel to place them in between the gap electrodes [43]. In spite of all these new innovative ideas to make CNT circuits, reduction in contact resistance remain as an important field of research. Contact resistance in the CNT circuits can be reduced by the exposure of electron beam. Electron beam induced deposition (EBID) has been used as solder material to create metal electrode at the CNT-electrode junctions [44]. Rapid thermal annealing has also been employed to reduce the contact resistance [45]. In the literature, researchers have showed the self-assembly of dropcasted CNTs across the gap electrodes using metal organic precursor [46]. The schematic of dropcasted CNTs across the electrodes is shown in Figure 1.5.

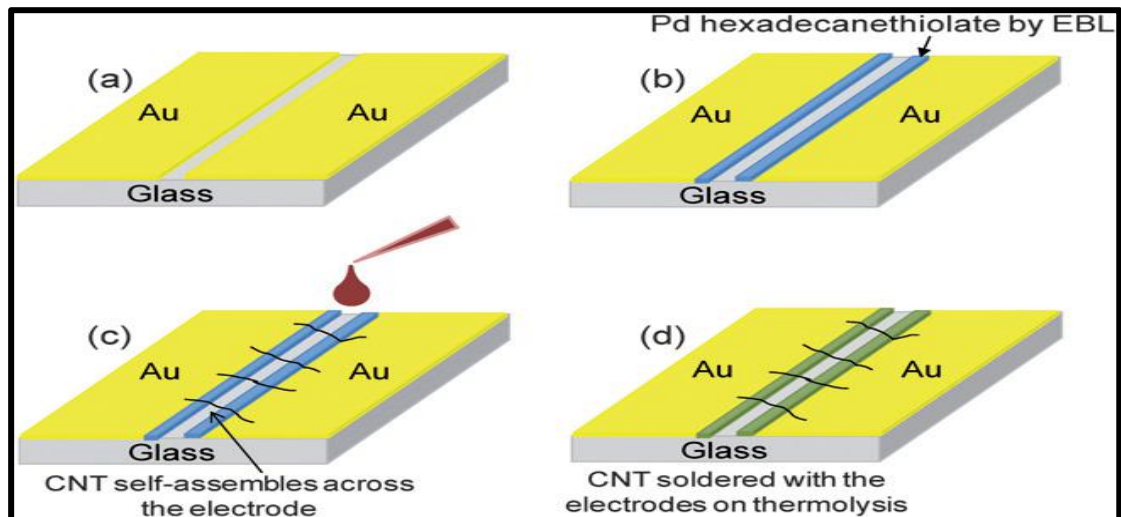


Fig 1.5 [46]: Schematic of (a) patterned gold electrodes. (b) metal organic precursor is patterned along the gold electrodes. (c) self-assembly of dropcasted CNTs. (d) Self-assembled CNTs are soldered via thermolysis.

1.4.3. Energy Storage Applications

Previous studies have shown the encapsulation of these transition metal oxides inside the carbon nanotubes for the high-performance lithium-ion batteries [47] [48]. CNTs provide large space for the volume expansion of encapsulated metal oxide nanoparticles and thereby improving the stability of electrode. Overall conductivity of the anode is increased as CNTs is acting as conducting layer and the formation of solid electrolyte interface film on CNT surface may decreases the capacity fading of anode [84]. Co_3O_4 nanomaterials have also been explored as high performance anode material for LIBs [49].

1.4.4. Spintronics Applications

Spintronics uses the spin of electrons in addition to its fundamental electronic charge which is the basis for electrical and electronic industry. During last couple of decades, gadgets utilizing spin degree of freedom have become commercially available. For instance, Spin Valves has been commercially used in our disk-drive read heads based on giant magnetoresistance(GMR) effect. In the literature, researchers were able to successfully transfer the spin information into large electrical signal using MWCNTs [50]. Transformation of spin signals to large electrical signal is restricted by spin relaxation and gives low value of magnetoresistive signals [51]. This spin relaxation has been seen to decrease by using MWCNTs as non-magnetic channel between highly spin polarized lanthanum strontium magnetite(LSM) at low temperature. This enhancement of performance is due to long spin lifetime and high Fermi velocity in CNTs [50]. The milestone of the digital age has been proposed in 1990 with the idea of fabrication of spin field-effect transistor which has the possibilities to go beyond the fundamental limitations of silicon based electronics [52].

1.4.5. Encapsulation of Magnetic Oxides inside CNTs

Ferromagnetic and antiferromagnetic transition metals and their oxides are crucial for spintronic based applications. Magnetic oxides exhibit novel functional properties but their preservation during device application has been an issue [74]. In addition to that, the integration of the magnetic metals and oxides with Si based semiconductor

industry is another practical issue [74]. Since the CNT can be both semiconducting and metallic and magnetic oxide can also be metallic, semiconducting or insulating, their integration is likely to provide a tool to tailor both electronic and magnetic properties of the hybrid structure. Ferromagnetic metals such as Fe have been successfully encapsulated inside CNT but Ni and Co have not been easy to encapsulate. Oxide encapsulation is even more rare and there exist few examples such as Fe_2O_3 [48], V_2O_5 [67] and Cr_2O_3 [74]. One approach in capturing magnetic oxide inside CNT is to first encapsulate the metal followed by its oxidation. Another approach is using capillary action [78]. In this work, we have first encapsulated a ferromagnetic metal inside CNT. This can be converted to metal oxide filled CNT by suitable annealing. Both type of samples can be used for spintronic based applications.

1.5. Plan of Thesis

In this work, we have attempted to encapsulate ferromagnetic metal Co inside CNT. This will be followed by the conversion of the encapsulate to various oxides like CoO and Co_3O_4 . Cobalt is known to be a stronger ferromagnet than Fe with Curie Temperature of 1388K [75]. Various oxides of Co have also functional properties that can be relevant to spintronic and battery applications. In some cases such as CoO whose Neel temperature is found near room temperature, which will be important for practical applications [76].

Aligned forest of CoMWCNTs exist in literature, however they have been grown by patterning a thin films of cobalt catalyst on a silica substrate [77]. In this thesis, we show that it is possible to grow very large (more 100 micro meter) aligned forest of CoMWCNTs with very good yield and reproducibility. We also show that these Co@CNT can be converted to Co oxide forest.

Chapter 2

Methods

2.1. Sample Preparation

Controlled growth of cobalt filled multi-walled carbon nanotubes (Co@CNT) were synthesized by thermal chemical vapor deposition (CVD) of cobaltocene mixed with camphor. CVD process is chosen because it provides a suitable route to bulk production of good quality nanotubes. Single zone furnace system were used to grow Co-filled MWCNTs. The respective amount of cobaltocene and camphor were thoroughly mixed in mortar & pestle and were further pelletized using a 10mm die in KBr press. Then the mixture were sublimated at about 200°C in the sublimation zone and the vapor was then transferred by a argon flow into the pyrolysis zone held constant at 800°C. Cobaltocene is acting as source of metal particle catalyst as well as source of carbon with extra carbon source provided by camphor. The mixture were finally decomposed in the pyrolysis zone and carbon nanotubes were deposited on the inner walls of quartz tube. After the reaction time of 10 min, furnace was switched off and cooled down to room temperature in the continuous argon flow. The detailed description of sample preparation is given in chapter 3.

2.2. Characterization Techniques

Field emission scanning electron microscopy (FESEM), Powder X-ray diffraction (P-XRD), Raman spectroscopy and Superconducting quantum interference device(SQUID) were used for the characterization of prepared sample.

2.2.1. Field Emission Scanning Electron Microscope(FESEM)

It is microscope which uses an electron to probe the surface of the specimen. These electrons are ejected by the field emission sources and having energy ranging from few eV to several KeV. These primary electrons accelerated within the high vacuum chamber and deflected by electronic lenses to produce narrow beam directed on to the sample. Electron beam interacts with atoms at various levels within the sample to produce different types of signal shown in Fig 2.1 [53].

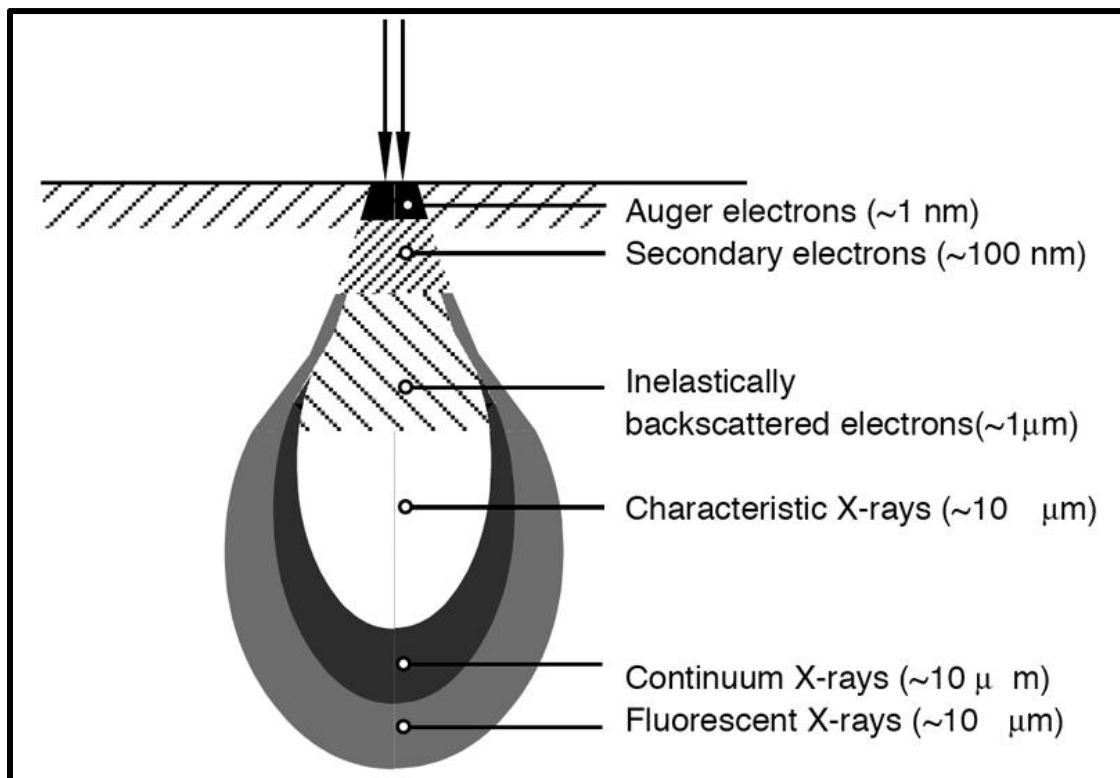


Fig 2.1 : Schematic of various electron-specimen interaction

Secondary electron imaging(SEI) is the most common mode of imaging specimen surface. Secondary electrons are ejected from thin specimen surface due to the inelastic scattering. The angle and velocity of secondary electrons are associated to surface structure of specimen. A detector collects the secondary electrons and convert it to the electronic signal. The small electronic signal is amplified and transformed to video scan image that is visible on computer screen. Prepared samples were imaged using Zeiss ultra plus scanning electron microscope(SEM). The point resolution can reach up to 0.4nm using the secondary electron detector [54].

2.2.2. Powder X-Ray Diffraction (P-XRD)

Its a powerful technique to do the structural analysis of materials. It works on the basic principle of X-rays diffraction from atoms. The X-rays are only diffracted when the distance between crystal planes is of the order of wavelength of X-rays. This condition is the famous Bragg's law which relates the wavelength of X-rays to the diffraction angle and lattice spacing in the sample. The detector records the signal and

converts it to the count rate which is output to the computer screen. Schematic of Bragg condition is shown in Fig 2.2 [55].

The samples used in this work characterized in the most common Bragg-Brentano geometry using Bruker D8 advance diffractometer with Cu- α (1.5404Å). The material to be analyzed should be finely powered and homogenized. The sample was scanned through the range of 10° to 80° with the step size of 0.0196°. All possible diffraction directions should be taken care due the random orientation of powered sample. The recorded spectrum was between intensity of X-rays and 2θ .

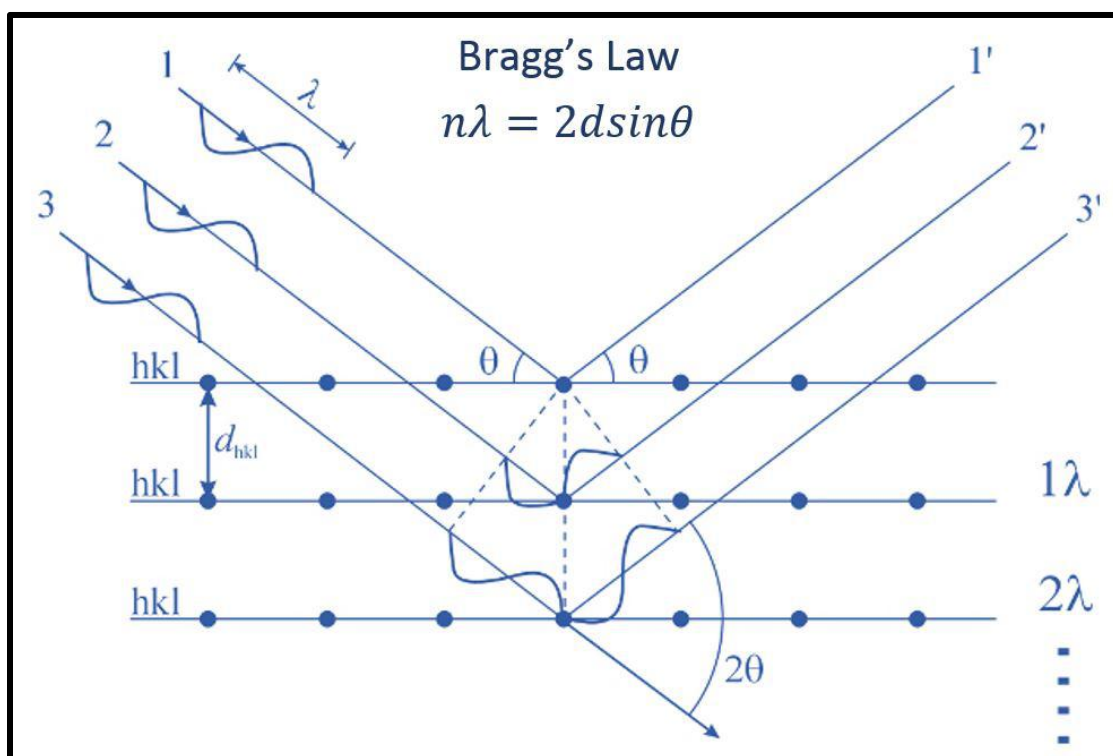


Fig 2.2 : Pictorial representation of Bragg's law

2.2.3. Raman Spectroscopy

Raman analysis has become an important characterization tool for carbon nanotubes. It tells us about the quality of tubes. Its a technique based on Raman effect in which the frequency of scattered radiation is different from incident monochromatic radiation. It relies on inelastic scattering and probes the molecular vibrations along with other low frequency modes in the sample. Change in polarizability is the essential condition for the Raman scattering. Most of the scattered radiation falls under Rayleigh scattering in which frequency of elastic scattered

radiation is similar to the incident laser radiation. These Rayleigh scattered light is filtered out by using band pass filter. Only small fraction of Raman scattered radiation is collected on to the detector. The different types of scattering is shown below in Fig 2.3 [56].

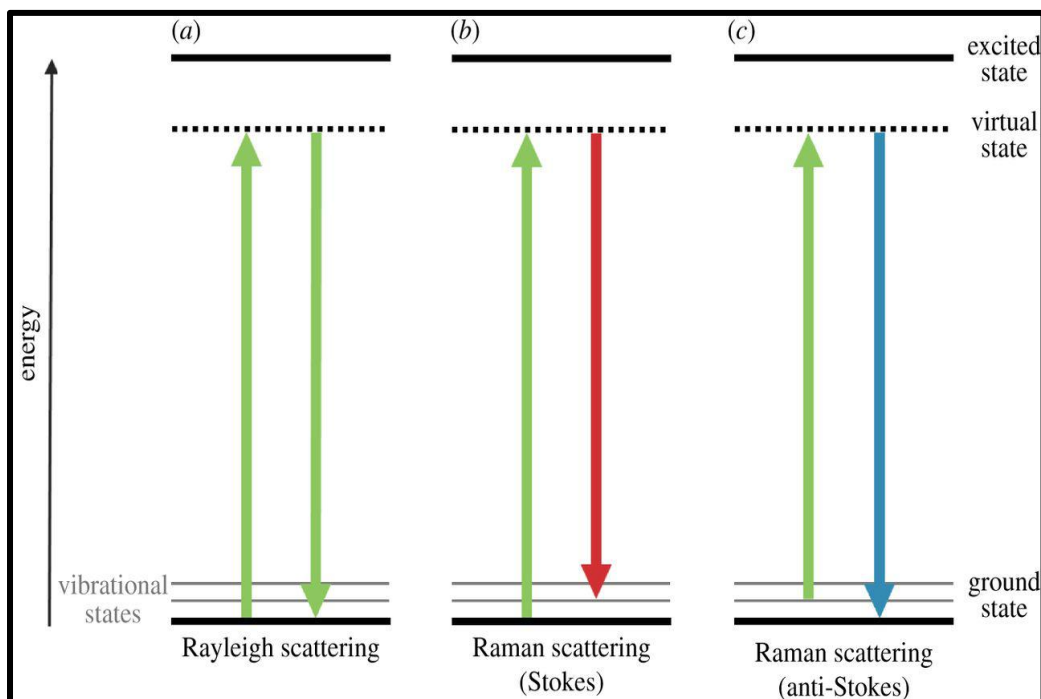


Fig 2.3 : Schematic of energy transition involved in Rayleigh and Raman scattering.

Charge-coupled device (CCD) is used as a detector. The sample is scanned through a range of 200 cm^{-1} to 3000 cm^{-1} and spectrum is recorded as an intensity Vs wave number. Raman measurement were carried out using blue laser of wavelength 488 nm at room temperature. Raman instrument used in this work is Olympus BX4, Horiba (Jobin Yovan).

2.2.4. Superconducting quantum interference device (SQUID)

Quantum Design Magnetic Property Measurement System (MPMS) were used to do magnetic measurement on the sample. It is a very sensitive magnetometer which is used to measure very small magnetic fields. It can measure as low as $5 \times 10^{-7} \text{ emu}$ based upon Josephson junction in superconducting loops [57]. Flux quantization and the Josephson effect are the two important properties utilized in the SQUID.

Non-magnetic capsule is used to hold the sample at the center of non-magnetic straw. Only 2.4 to 2.5 mg of sample were used due to limited amount of sample. Then the non-magnetic straw is inserted inside the chamber which contains superconducting pick up coils. The chamber is evacuated by purging it several times before taking measurements. A current starts flowing in the loop whenever there is a change in magnetic flux. This current is converted to output voltage which oscillates with the change in phase at Josephson junction and this change in phase, in turn, depends upon change in magnetic flux. Finally the calibrated device converts the output voltage in magnetic moment and plots a graph between magnetic moment vs applied field. A schematic of sample placed in between pick up coils is shown in Fig 2.4 [58].

In this work, room temperature $M(H)$ has been done on the sample in the range of -50K Oe to 50 KOe using Qunatum Design MPMS XL.

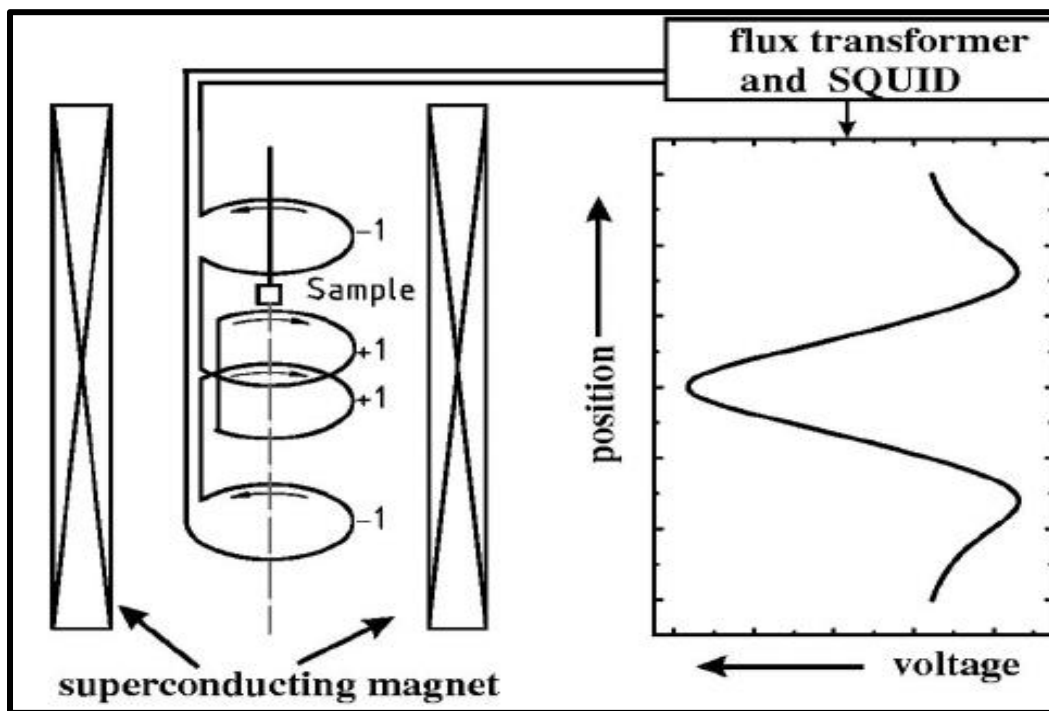


Fig 2.4 : Schematic showing sample between the pick up coils and theoretical response signal due to change in magnetic flux.

Chapter 3

Cobalt-filled@CNTs

Synthesis and Characterization

In this chapter, the synthesis and characterization of aligned forest of Co@CNT is presented. The experimental set up used for the synthesis has been described in details. The crucial factors for the formation of aligned forest have been highlighted. The electron transport and magnetic properties have also been investigated.

3.1. Schematic of the CVD set up:

Usual technique of CVD which is widely used to synthesize Fe filled CNT by pyrolysis of metallocene has been used here with some modifications. This technique uses a two zone furnace with two independent temperature controllers for sublimation and pyrolysis. However the setup used in this work uses a single zone furnace with long constant region. A compression seal arrangement has been used to transfer the metallocene in the sublimation zone. This arrangement provides access to find a sublimation point, from the varying temperature zone of the furnace. The details of this setup are discussed in reference [73]. The schematic is shown in Figure 3.1 with all important details related to set up.

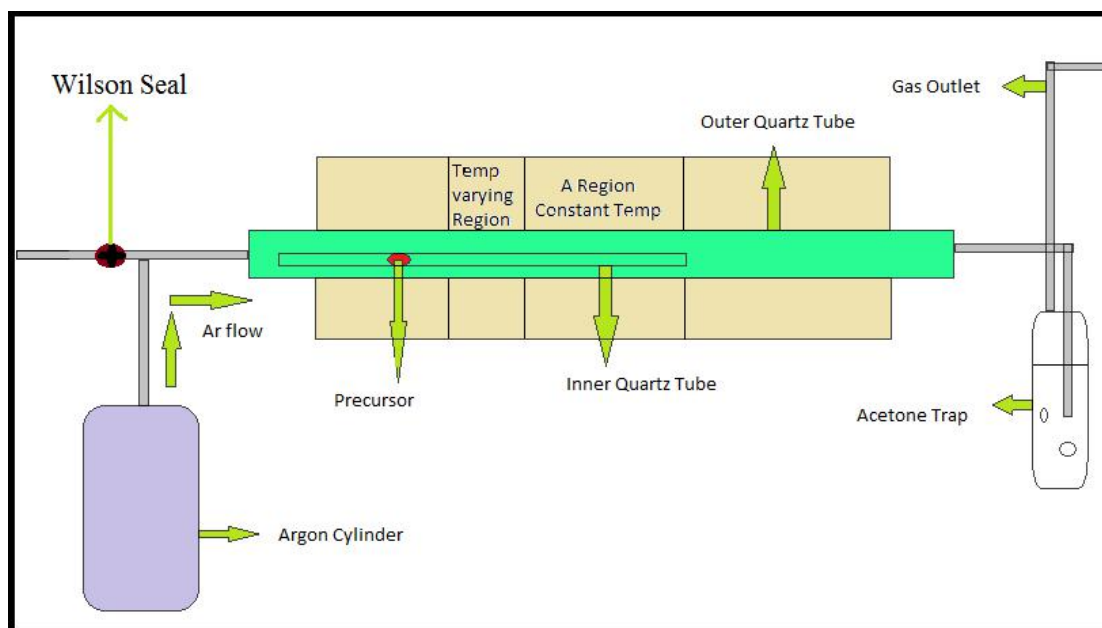


Fig 3.1 : Experimental set up used for the synthesis of Co@CNT.

3.2. Use of Camphor with Cobaltocene:

As mentioned previously, it is relatively easier to form Fe filled CNT by using this technique. However the formation of Ni and Co filled CNT, especially their aligned forests have been difficult. We also could not obtain good quality Co@CNT by pyrolysis of cobaltocene. However addition of camphor, which is a environment friendly green material enabled us to obtained highly aligned forests of Co@CNT. Though camphor has been used to obtain pristine CNT by using zeolites [79] but to the best of our knowledge Co filled CNT have not been formed using the combination of camphor and cobaltocene.

The optimized parameters for successful runs is discussed in the following. Cobaltocene mixed with camphor in the ratio of 5:1 by weight for the synthesis of vertically aligned Co@CNTs with the diameter of 40-70nm and length 6-20 μ m. Co@CNTs were synthesized by using CVD method in single zone horizontal tube furnace(Nabertherm RHTH 120/300/16) of length 158 cm and 7 cm in diameter.

There are four important experimental parameters, which include sublimation temperature (T_s), pyrolysis temperature (T_p), argon flow rate and amount of cobaltocene. These four parameters are usually optimized for getting best aligned forest structure. In this case, the fifth parameter is the amount of camphor. At the optimized T_s , both cobaltocene and camphor were sublimed. In our experiment, the

optimized T_s is 200°C . After optimizing T_s , different T_p were tried. At T_p , 900°C , evidence of tubes depositing on quartz substrate was very less. However the best results were obtained for 800°C . Amount of precursor was also optimized after optimizing T_p and T_s . (Table 3.1)

Another important parameter to be optimized is flow rate of argon gas which is used as a carrier of sublimated fumes to the pyrolysis region. In the pyrolysis region, the sublimated fumes decomposes and finally Co filled CNT are deposited on the walls of quartz tube. (Table 3.2)

The prepared samples were imaged using Zeiss ultra plus scanning electron microscope (Figure 3.2, 3.3, 3.4 &3.5). The Energy Dispersive X-ray analysis(EDX) shows a peak for both carbon and cobalt. (Figure 3.6)

Amount of precursor	Ratio	Sublimation temperature	Pyrolysis temperature	Ar flow	Result
Cobaltocene=45mg Camphor=155mg	3:10	200°C	800°C	7 b/s	No evidence
Cobaltocene=500mg Camphor=100mg	5:1	200°C	800°C	7 b/s	Good evidence

Table 3.1 : Role of amount of precursor in determining aligned nanotubes

Amount of precursor	Ratio	Sublimation temperature	Pyrolysis temperature	Ar flow	Result
Cobaltocene=500mg Camphor=100mg	5:1	200°C	800°C	9 b/s	No evidence
Cobaltocene=500mg Camphor=100mg	5:1	200°C	800°C	7 b/s	Good evidence

Table 3.2 : Role of Argon flow rate in determining aligned tubes

3.3. SEM Results:

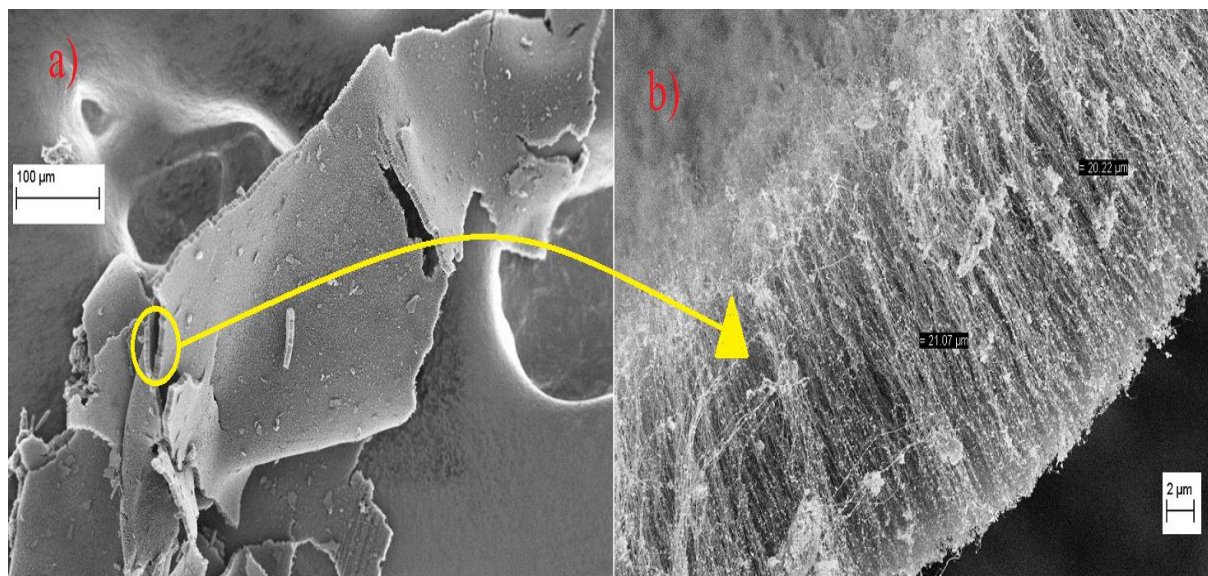


Fig 3.2 : SEM image of (a) aligned forest structure of cobalt filled CNTs formed in the constant temperature zone. (b) Zoom in image of aligned tubes of length approx 21μm

The above SEM image is showing that *as-prepared* Co@CNT. The parameters need to be optimized further for enhancing the yield. However the best results are fairly reproducible and the sample thus obtained contains very long (about a few 100 micrometer of length as is evident from Figure 3.2(a) aligned forests. The length of individual CNT in this case is in the range of 5-20 μm and the diameter is 30-70 nm. The carpet like structure in case of Co@CNTs were synthesized by pyrolysis of cobaltocene at 900°C [59].

The successful run gives yield in reasonable quantity for the basic characterization like XRD, SEM and Raman.

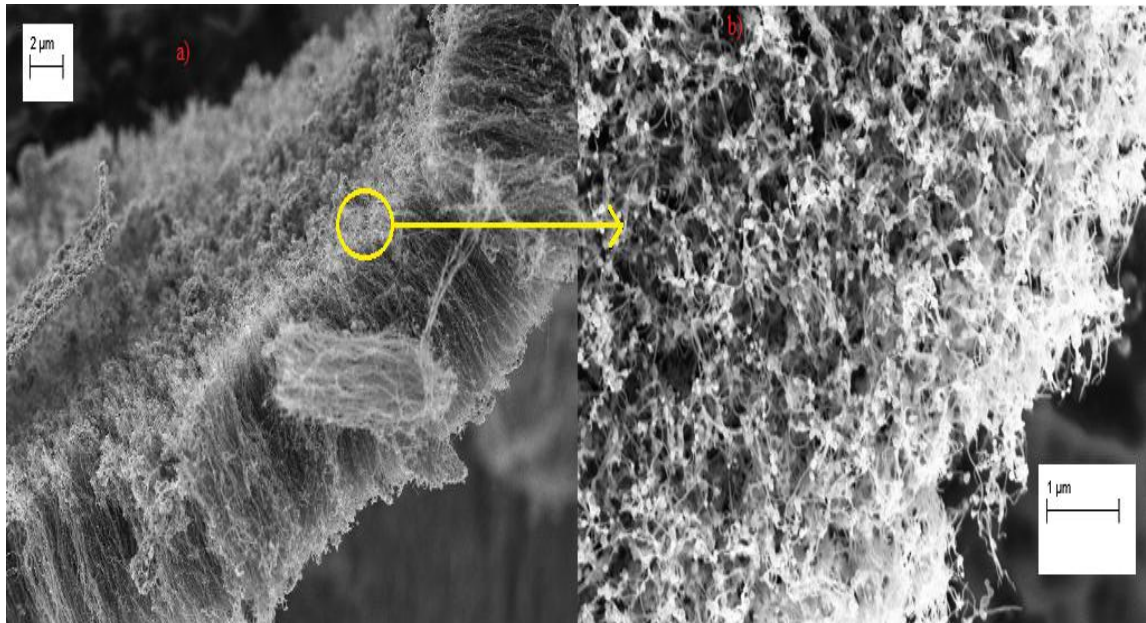


Fig 3.3 : SEM image of a) aligned Co@CNTs carpet. b) top view of aligned carpet. Both a and b sample were collected from constant temperature zone.

The above SEM image of cobalt filled tubes has moderate number of particles sticking on the surface wall of CNTs. These catalyst particles are usually sticking to CNT when pyrolysis of metallocene technique is used. However, these particles outside the CNT can interfere with the magnetic measurements. We have made attempts to reduce the density of such particles by increasing the amount of camphor. However, more experiments are needed to tackle this issue.

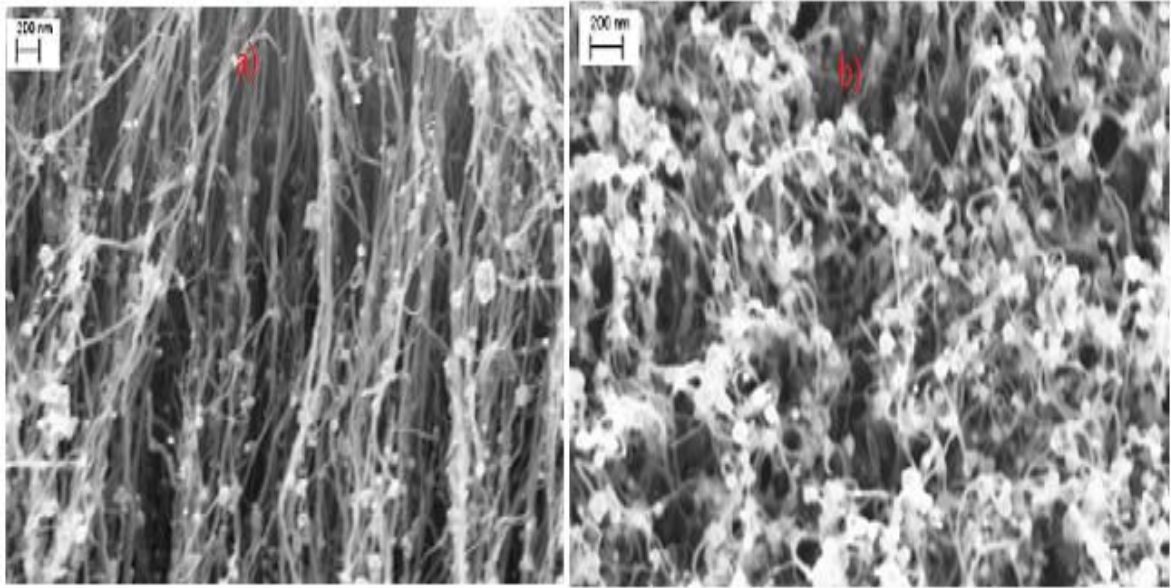


Fig 3.4 : SEM image of (a) aligned tubes with particles sticking on its surface. (b) top view of particles sticking on its upper end of aligned tubes. Both formed in constant temperature zone.

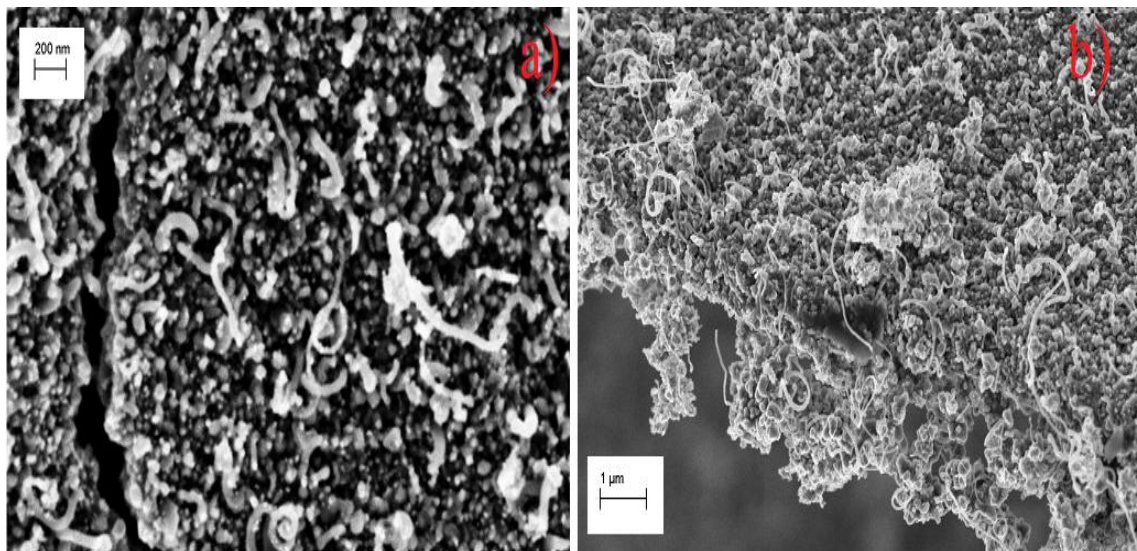


Fig 3.5 : SEM image of (a) few short length tubes with mostly particles. (b) randomly oriented nanotubes with large number of particles. Both a and b were formed in varying temperature zone.

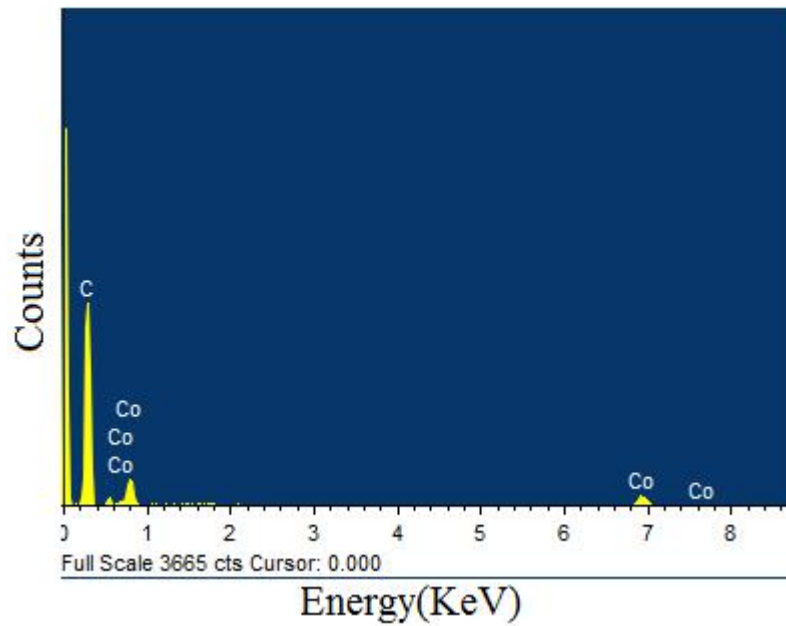


Fig 3.6 : EDX of CoMWCNTs using Zeiss ultra plus SEM with peaks of Co and C.

The growth process of Co@CNT is self organization. The role of camphor is to supply extra source of carbon for the growth of graphitic walls of CNT. The cobalt atom in the unit cell of cobaltocene provide the seed for the growth of Co filled CNT. Apart from the amount of Co and C in the precursor, the growth of Co filled CNT depends on the surface area of quartz tube. This portion of the quartz tube also needs to be in constant temperature zone. The area where temperature is seen to vary results in the formation of CNT with more catalyst particles or undesirable phases of amorphous carbon and cobalt (Figure).

The process of formation of CNT appears to be fast once the cobalt particle seeds reach the pyrolysis zone (region A in schematic). The other effective metal catalyst other than cobalt are iron and nickel [60]. These metals have the property to form ordered carbons due to their catalytic activity for the sublimed carbon compounds and the fact that carbon is able to diffuse over metal catalyst very rapidly [61] [62] [63]. The formation of CNT is possible only in the close proximity to the metal surface. When some other prominent reaction happens away from the metal surface that can leads to the formation of unwanted amorphous carbon products. These reaction can be restricted depending on the choice of carbon precursor and reaction temperature.

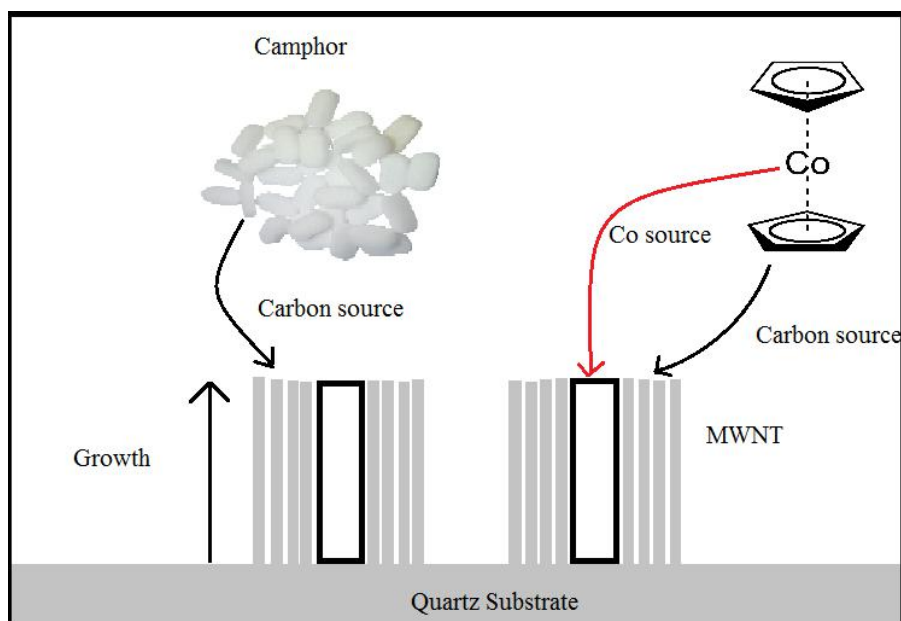


Fig 3.7 : Schematic of feedstock of Co and Carbon to MWNT growth

3.4. Powder X-ray Diffraction

The powder XRD data for CoMWCNTs shows the graphitic peak at $2\theta = 25.64^\circ$. The cobalt oxide (CoO) major peaks were found at $2\theta = 36.29^\circ$, 42.15° and 61.15° . These CoO diffraction peaks were compared to the JCPDS pattern number 01-078-0431. The Co_3O_4 peaks were found at $2\theta = 31.07^\circ$, 55.58° , 65.05° and 68.84° . These Co_3O_4 peaks were compared to JCPDS pattern number 00-042-1467. The peaks corresponding to α phase of cobalt were also found in the spectrum. The peak position for α phase cobalt at the respective $2\theta = 44.03^\circ$, 51.39° , 75.72° and these diffraction peaks were compared with JCPDS pattern number 00-015-0806. By comparing these results to the JCPDS data cart, each peaks were correctly identified corresponding to constructive interference of Bragg reflected rays.

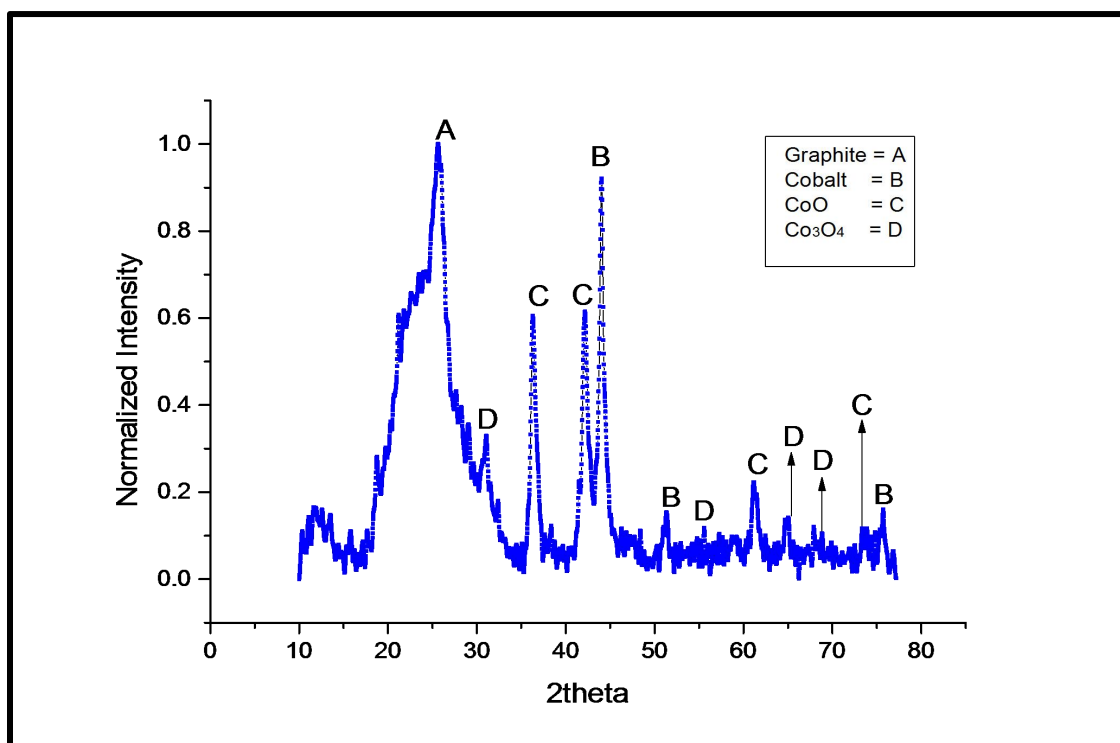


Fig 3.8 : XRD of Co@CNTs with graphitic and cobalt oxide peaks

3.5. Raman Spectroscopy

Raman spectroscopy is an important characterization technique for both multi-walled and single-walled carbon nanotubes. Raman peaks provides a direct molecular fingerprint of the molecules being observed. Raman measurement were done using blue laser at room temperature.

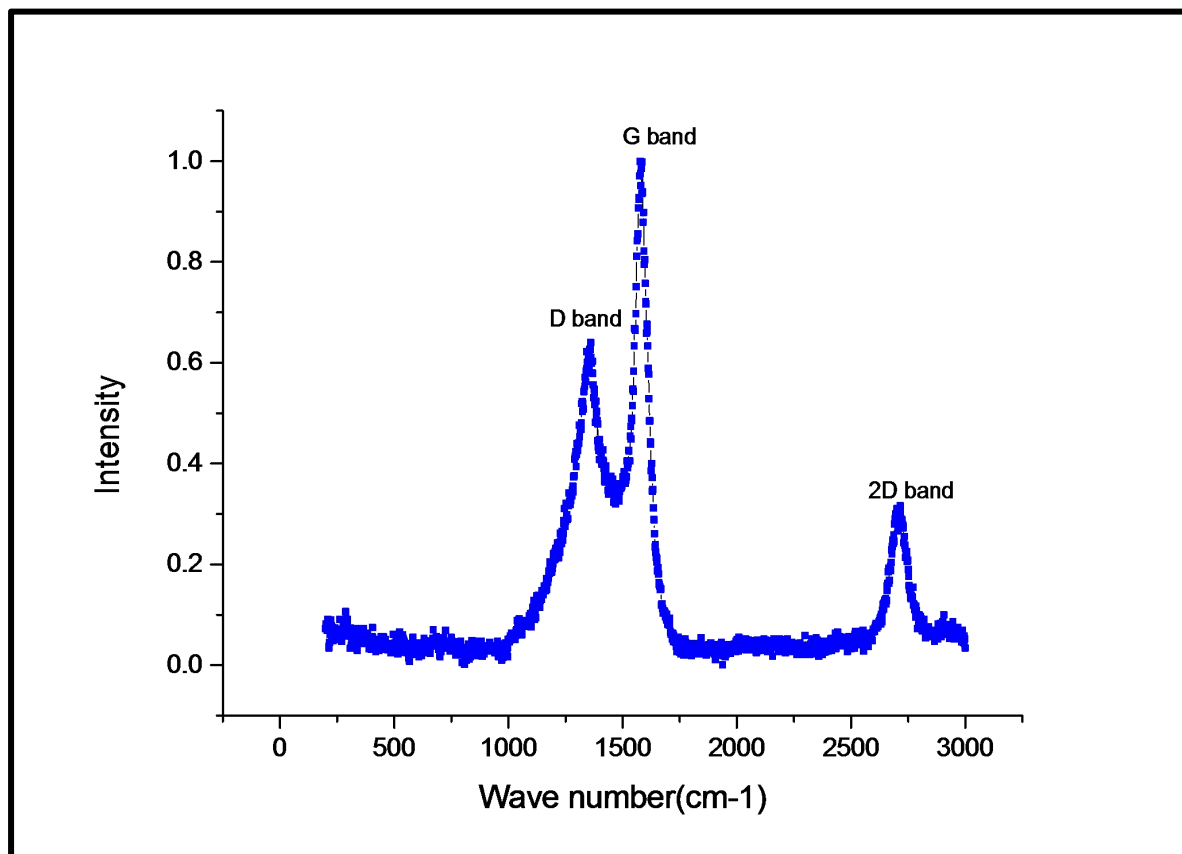


Fig 3.9 : Raman spectrum of CoMWCNTs with well defined D and G bands.

The I_d/I_g ratio of D and G band is 0.639. In the raman spectrum, the G band appears around 1576.71 cm^{-1} is the first-order Raman peak. This G band assign to the in-plane vibration of C-C bond. There also exist the D band which is activated due to the disorder present in the system being observed. This defect induced band involved double resonant scattering processes in which electrons are elastically scattered by structural defects. In the spectrum, the D band appears around 1360.61 cm^{-1} . The spectrum contain another band called the G' band appears at 2714.97 cm^{-1} and assigned as the overtone of the D band.

3.6. Magnetic measurements

The magnetization of Co@CNT was measured at room temperature using a SQUID detector which is able to detect magnetic moments up to 10^{-7} emu. The graph is plotted between magnetic moment(emu) and applied field(B). The sample exhibits a magnetization of 9.4 emu/g and a coercive field of approximately 660 Oe.

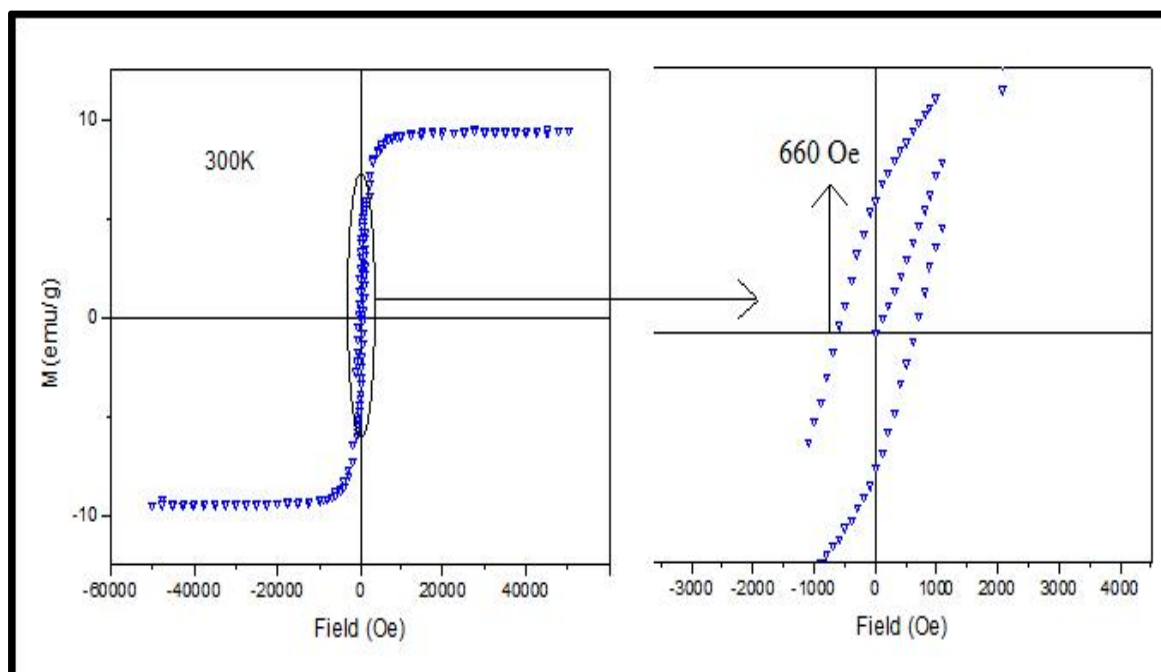


Fig 3.10 : Hysteresis loop for the aligned CoMWCNTs at room temperature.

The saturation moment of 9.4 emu/g is consistent with the previous magnetization studies done on cobalt-filled CNTs [64]. This value of saturation moment is close to reported value for cobalt nanoparticles [65].

3.7. Electron Transport Measurements

I-V measurement of the bulk sample has been done by drop-casting the sample in between the two gold electrodes. The sample is dispersed in ethanol and sonicated for about 1min before drop-casting. The two gold electrodes of thickness approximately 50nm were coated on glass slab by sputter coating. Then two copper wires were gently soldered on to the gold electrodes. These copper wires were then connected to source meter by using alligator clips.



Fig 3.11 : (a) I-V measurements were done using source meter. (b) inset: Co@CNTs were dropcasted between two gold electrodes.

The electron transport measurement were done using Keithley Source meter 2450. The picture of source meter is shown in Figure 3.3 with the inset showing dropcasted sample in between the Au electrodes.

The measurement were done using sweep mode in source meter by defining the voltage ranges and the maximum current that can pass through the sample. The CNT circuit which is fabricated between the Au electrodes is acting as a resistors. It is important to be aware of maximum current passing through the sample to avoid the damaging of CNT. The CNTs can undergo temperature rise, if higher current passes through CNT circuit [46].

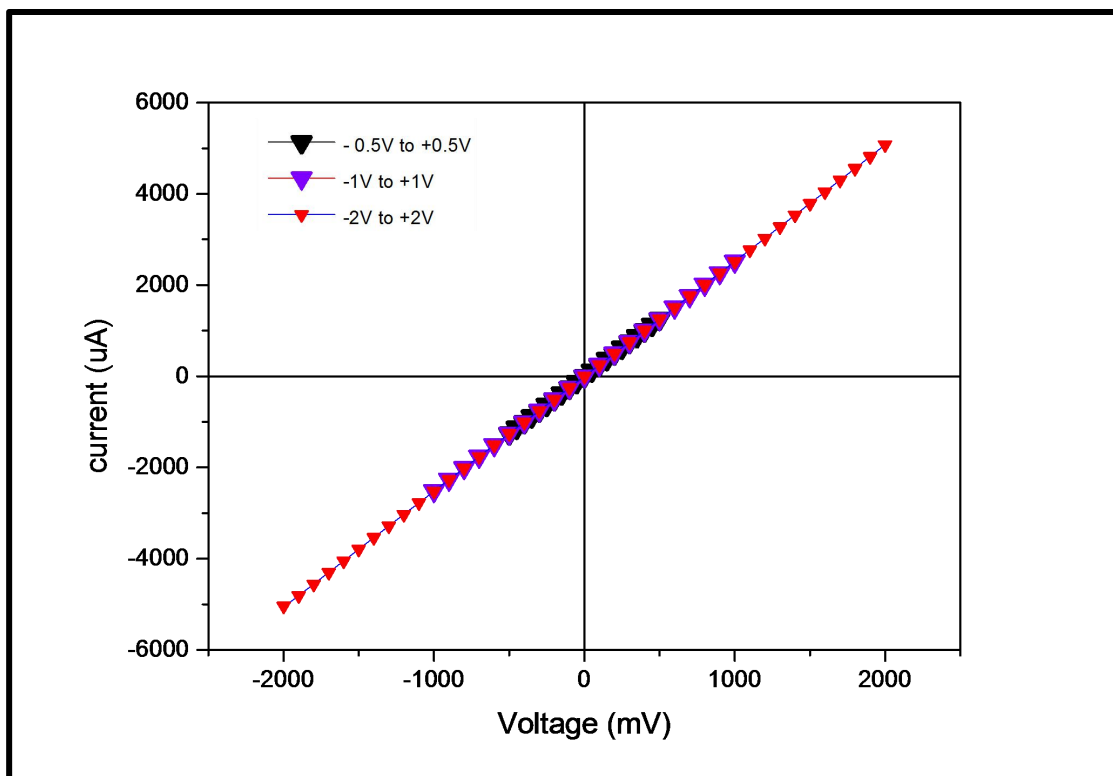


Fig 3.12 : I-V characteristics of bulk CoMWCNTs across the Au electrodes

The graph is plotted between voltage (mV) on x-axis and current (μA) on y-axis. As it is clear from the Figure, I-V curve shape is linear with the resistance of approximately $\sim 400 \Omega$.

Chapter 4

Conversion of the aligned forest of Co@CNT to CoO_x

Synthesis and Characterization

In this chapter, the oxidation of Co@CNT is presented. This procedure can result in two types of sample. First is the sample in which the encapsulate (Co) is converted to CoO_x, in which the graphitic shells of CNT are retained. In the second possibility, another type of sample can be only the aligned forest of CoO_x where graphitic shells can be completely removed by the oxidation procedure. Since CoO_x can exist in various valence states, it requires optimization of parameters to form an oxide with particular valence state. Experimental parameters during oxidation need to be optimized for obtaining two types of samples.

We have successfully converted the Co filling to Co₃O₄, while retaining the aligned forest structure. The characterization using SEM, XRD and Raman is presented in this chapter.

4.1. Oxidation of Co@CNT

Cobalt filled tubes were oxidized in the same furnace (used for Co filled tubes synthesis) at 500°C in the presence of continuous CO₂ flow.

The sample for oxidation was prepared by taking a small amount (approx 1 mg) of cobalt filled tubes into ethanol solution. The sample was dispersed uniformly by sonicating it for a few seconds. Thereafter, the dispersed tubes were drop-casted onto the quartz slab, which was placed inside the furnace. The sample was slowly heated up to the temperature of 500°C and kept at this temperature for about 10 minutes. During this heat treatment, the continuous flow of CO₂ was maintained. The furnace was switched off after 10 minutes and the CO₂ flow was retained till the temperature drops down to 200°C. CO₂ was chosen instead of O₂ because by optimization of the annealing temperature, both CoO_x@CNT as well as only CoO_x can be obtained.

Presently, we have obtained aligned forest of CoO_x nano wires by completely removing the graphitic shells.

After cooling down to room temperature, the oxidized sample were collected and morphological analysis were done by SEM. The elemental composition were confirmed through EDX. The structural analysis were done by XRD. Raman analysis also confirms the existence of cobalt oxide in the the sample.

4.2. SEM images

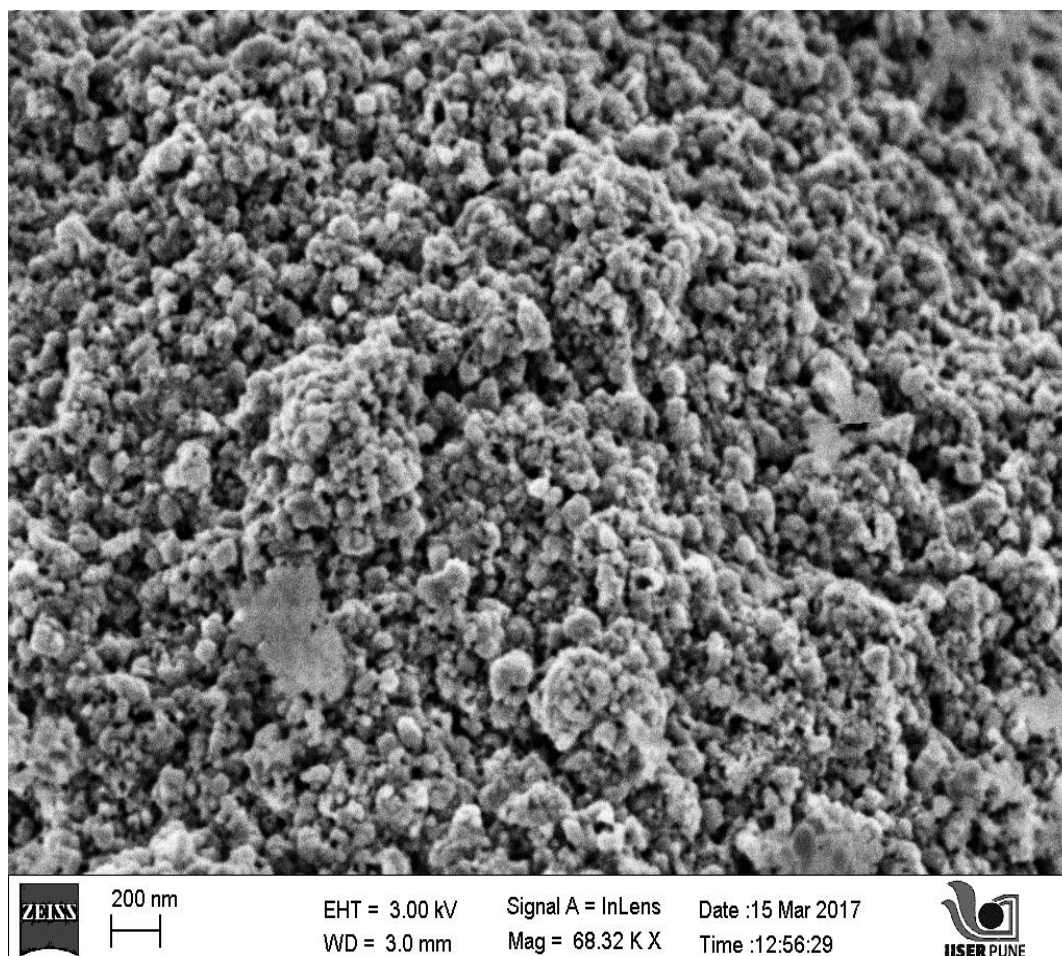


Fig 4.1 : SEM image of oxidized sample with no evidence of tubes.

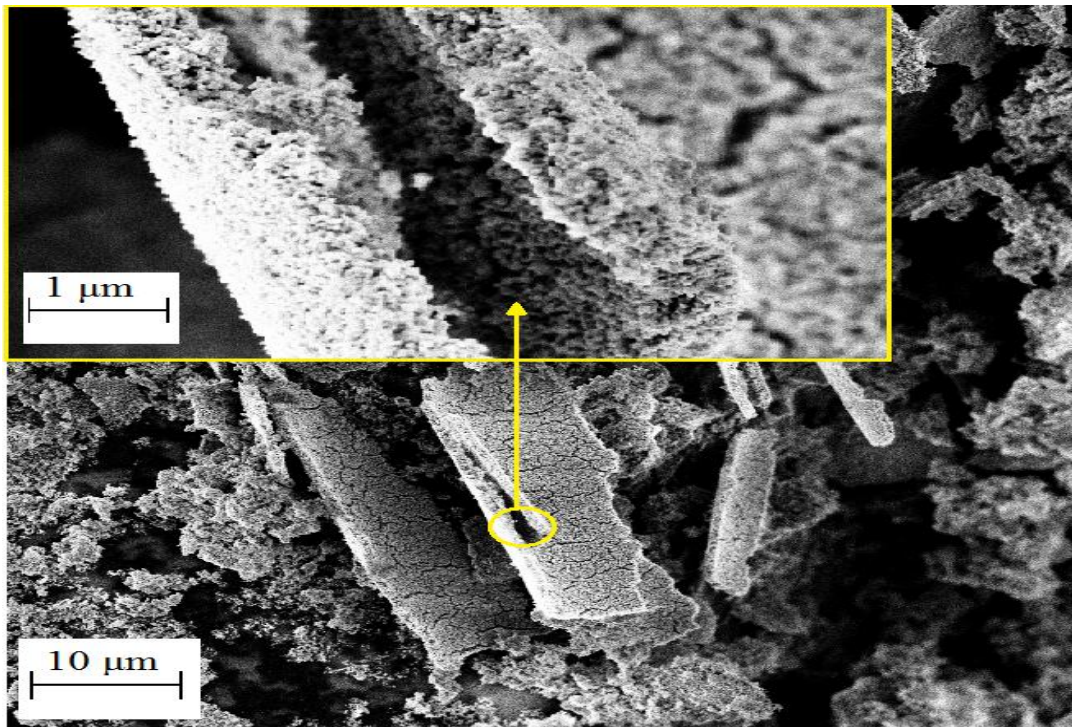


Fig 4.2 : Forest structure has preserved after the oxidation treatment.

The SEM image shown in Figure 4.1, has large number of cobalt oxide particles. From Figure 4.2, it is clear that the forest structure of Co filled tubes is still preserved even after oxidation treatment. In the figure 4.3, comparison has been made to show the preservation of forest structure even after the oxidation treatment. Three things happened during oxidation. First, filled cobalt particles converted to Co_3O_4 , second, carbon shell were burned off but forest structure remained preserved and third, CoO which were present before oxidation were converted to Co_3O_4 after oxidation. As it is known that CoO is not stable if heated in the presence of air [72].

There is a need of optimizing the oxidation temperature for carbon shell to be preserved. Previous studies have shown that higher oxidation temperature leads to loss of larger proportion of nanotubes [66]. There is another important parameter which can affect the preservation of carbon shell is the flow of CO_2 during oxidation. Fe@CNT has been successfully converted to FeO_x encapsulated within CNT without the loss of carbon shell [73].

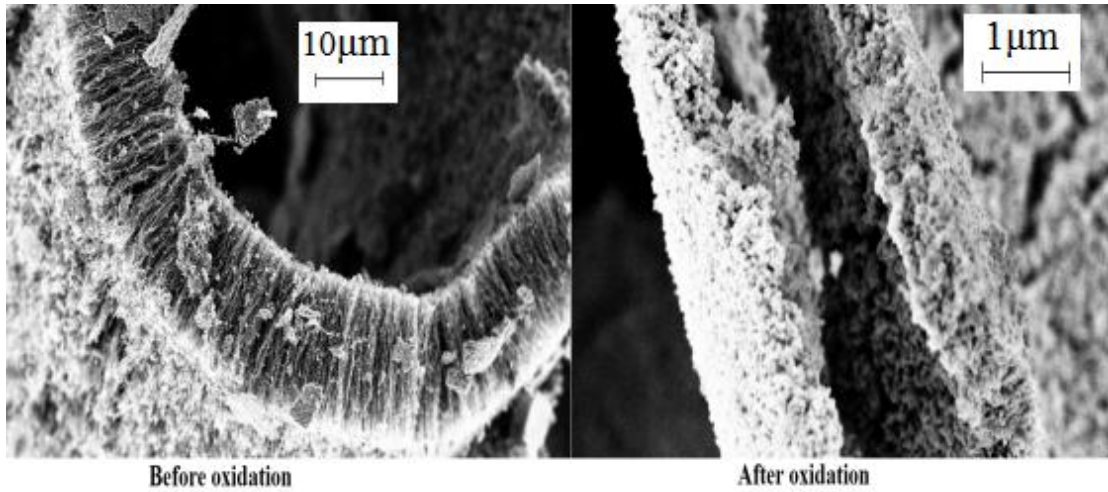


Fig 4.3 : Comparison been made between forest structure before and after oxidation.

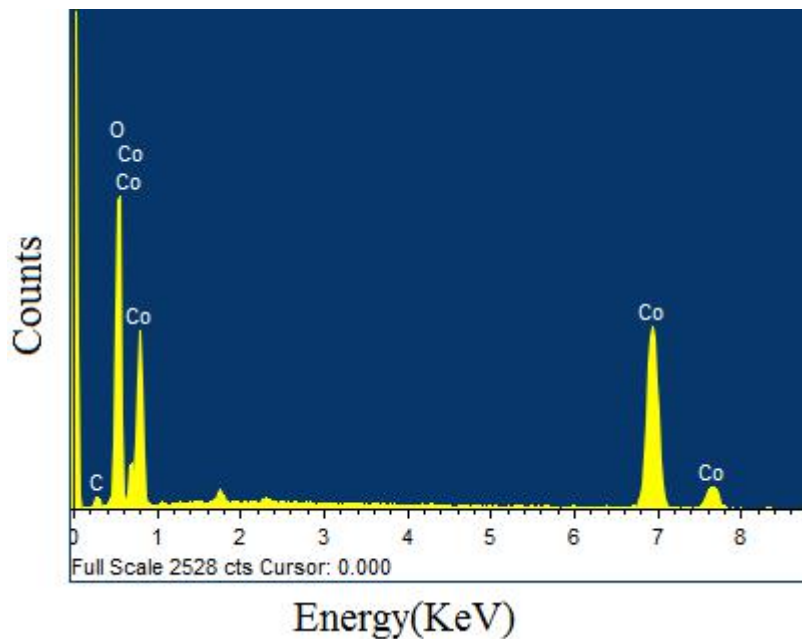


Fig 4.4 : EDX of Oxidized sample with the major peaks of Co and O

The Figure 4.4 shows the elemental confirmation of oxidized sample with a major peaks of cobalt and oxygen. There is also a small percentage of carbon in the obtained sample after oxidation. Since Co can exist in various valence states, forming different type of oxides which can have different magnetic transition temperatures. However it is difficult to determine exact oxidation state using EDX as it is not a sensitive technique for determination of oxygen . However magnetic measurements along with

XRD and Raman (given in the next section) are needed to confirm the the presence of the exact oxide. Our XRD data shows the presence of Co_3O_4 . Magnetic measurements are yet to be conducted to determine the magnetic transition temperature. In table 4.1, the magnetic transition temperatures of Co metal and its various oxides, that can possibly exist inside the CNT are given. We intend to stabilize various CoO_x oxide inside the CNT and also perform magnetic measurements to further confirm the magnetic state of the encapsulate.

Material	Type	$T_c(\text{k})$	$T_n(\text{k})$	Reference	Year
Co	Nanoparticle	10		[80]	2009
Co	Bulk	1388 ± 2		[81]	1965
CoO			293	[82]	1956
Co_3O_4	Nano-wire		23.7	[83]	2010
Co_3O_4	Macroscopic crystal		40	[83]	2010

Table 4.1 : Magnetic transition temperature of Co and its oxides.

4.3. Powder X-ray Diffraction

The diffraction analysis of oxidized sample has revealed the full conversion of Co@CNTs shell into cobalt oxide (Co_3O_4). The graphitic shell of CNTs were burned off while oxidizing the Co-filled CNTs at 500°C . The graph is plotted between 2θ on x-axis and intensity on y-axis (Fig 4.3).

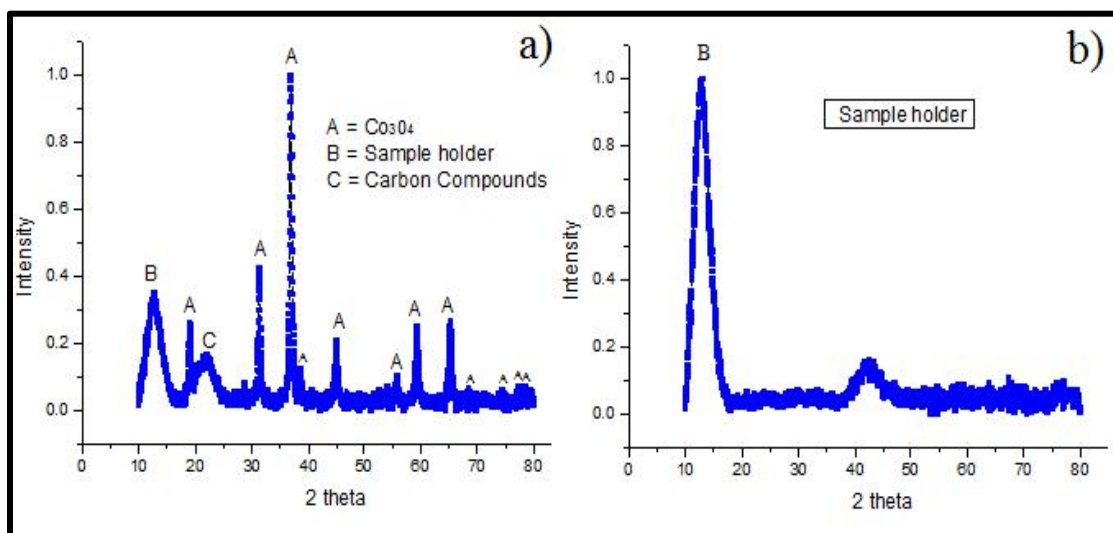


Fig 4.5 : XRD pattern of (a) Oxidized sample (b) only sample holder

These diffraction peaks were perfectly indexed to the cubic spinel structure of Co_3O_4 with lattice parameter $a = 8.08\text{\AA}$, consistent with the JCPDS pattern number 00-042-1467 [68]. The XRD pattern in Figure 4.3 (a) clearly shows no evidence of peak corresponding to graphitic shell after oxidation. The peak, B, in Figure 4.3 (a) corresponds to sample holder. This has been confirmed by XRD measurement of sample holder separately (Figure 4.3 (b)). These obtained oxide were mixed valence compounds and could also be written as $\text{Co}^{\text{II}}\text{Co}^{\text{III}}_3\text{O}_4$ [69]. Electron energy loss spectroscopy (EELS) needs to be done to determine the different oxidation state present in Co_3O_4 .

4.4. Raman Spectroscopy

The Raman measurement of oxidized sample were done using blue laser of wavelength 488nm at room temperature. The graph was plotted between wave number on x-axis and intensity on y axis.

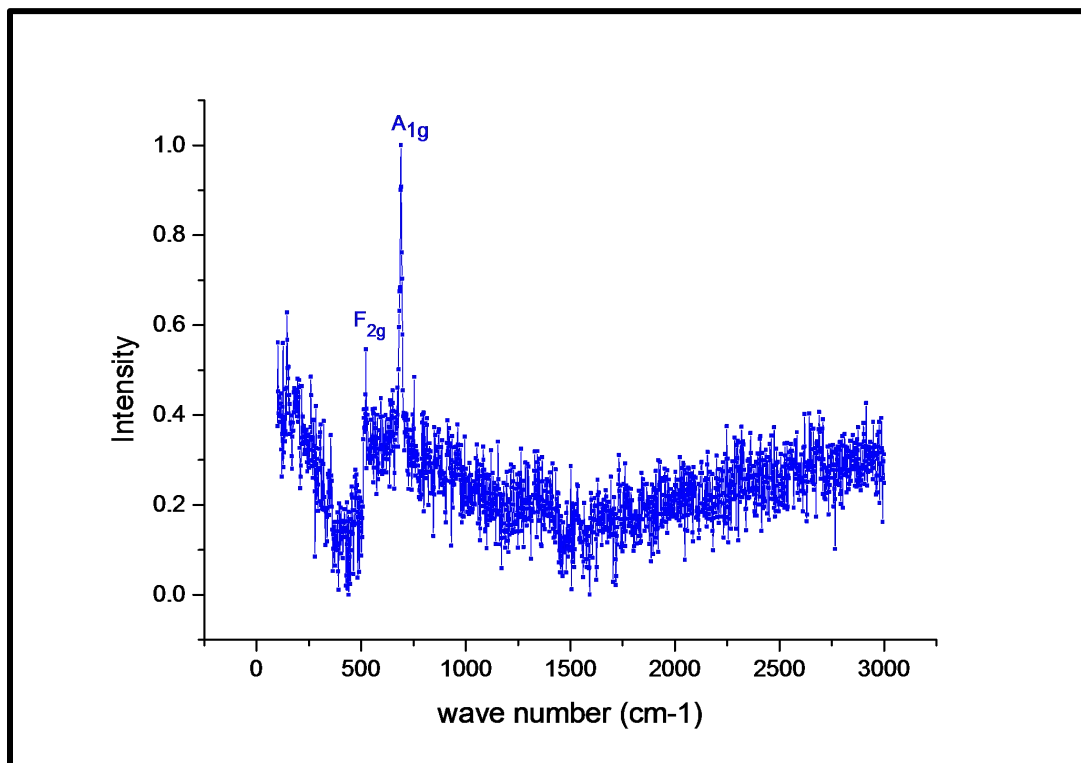


Fig 4.6 : Raman spectrum of oxidized sample with two Raman active modes.

In the previous studies, there were total of five Raman modes of Co_3O_4 which are active [70]. In case of oxidized sample, only two Raman active modes namely A_{1g} at 689.7 cm^{-1} and F_{2g} at 523.1 cm^{-1} which were consistent with pure crystalline Co_3O_4 particles [71]. However, due to the small amount of sample quantity, the data presented in Figure 4.4 is noisy and the measurement needs to be repeated with better statistics.

Chapter 5

Summary And Future Work

5.1. Summary

Cobalt filled multi-walled carbon nanotubes have been successfully prepared using the chemical vapor deposition method. The SEM images showed good quality of forest structure formation of aligned carbon nanotube by using cobaltocene in combination with an environment friendly compound camphor. XRD analysis showed the presence of α phase of face-centered cubic cobalt encapsulated within the graphitic shell and also shows the evidence of face-centered cubic CoO and Co₃O₄, which are likely to exist outside the CNT. Raman analysis has been successfully done on Co@CNTs and found well defined G band and D bands. Magnetic measurements showed the magnetization value of 9.4 emu/g.

The aligned forest of Co@CNTs have been successfully converted to aligned forests of Co₃O₄. SEM images showed that the preservation of forest structure after oxidation. Raman analysis showed the presence of two Raman active modes consistent with the pure crystalline Co₃O₄ particles.

5.2. Future Plans

In case of aligned forest of Co@CNTs, good quality aligned tubes has been prepared. However a large number of of unwanted cobalt nano particles sticks to the outer surface of nanotubes. The amount of camphor added to the cobaltocene precursor needs to be optimized to get rid of the unwanted cobalt particles. Structural analysis through Rietveld refinement of the prepared sample has to be done.

In case of CoO_xCNTs, more number of experiments to optimize the parameters need to be carried out for obtaining CoO_x@CNT. Temperature variation of pressed pellets of Co@CNT will enable us to understand the conduction mechanism in these hybrid structures and such measurements are planned to work out in future. Various type of nano spintronic devices can be fabricated using these Co and CoO_x@CNT. For the patterning of device lithography technique will be used.

References

1. Iijima, S., "Helical microtubules of graphitic carbon", *Nature*; 354(6348); 56-58. (1991).
2. Wang, X.; Li, Qunqing; Xie, Jing; Jin, Zhong; Wang, Jinyong; Li, Yan; Jiang, Kaili; Fan, Shoushan (2009). "Fabrication of Ultralong and Electrically Uniform Single-Walled Carbon Nanotubes on Clean Substrates". *Nano Letters*. 9 (9): 3137–3141.
3. Tenne R, Margulis L, Genut M, Hodes G (1992). "Polyhedral and cylindrical structures of tungsten disulphide". *Nature*. 360 (6403): 444–446. doi:10.1038/360444a0.
4. R. Saito, G. Dresselhaus, and M. S. Dresselhaus, *Physial Properties of Carbon Nanotubes*. London: Imperial College Press, 1998.
5. S. Bandow, S. Asaka, Y. Saito, A. M. Rao, L. Grigorian, E. Richter, and P. C. Eklund, "Effect of the Growth Temperature on the Diameter Distribution and Chirality of Single-Wall Carbon Nanotubes," *Physical Review Letters*, vol. 80, pp. 3779, 1998.
6. Wang, X.; et al., "Fabrication of ultralong and electrically uniform single-walled carbon nanotubes on clean substrates", *Nano Letters*; 9(9); 3137-3141. (2009).
7. Hongliang Zhang, Bin Wu, Wenping Hu and Yunqi Liu, *Chem. Soc. Rev.*, 2011, 40, 1324–1336.
8. M. Meyyappan, *Carbon Nanotubes Science And Application*. CRC Press LLC, 2005.
9. B. Bhushan, *Springer Handbook of Nanotechnology*: Springer - Verlag, 2004.
10. Peter J. F. Harris, *Carbon Nanotube Science*: Cambridge University Press, 2009.
11. S. Iijima, T. Ichihashi, *Nature (London)*, 363 (1993), p. 603.
12. Oxana V. Kharissova and Boris I. Kharisov*, *RSC Adv.*, 2014, 4, 30807–30815.
13. K. B. K. Teo, C. Singh, M. Chhowalla et al., 'Catalytic synthesis of carbon nanotubes and nanofibres', in *Encyclopedia of Nanoscience and Nanotechnology*, vol. 1, ed. H. S. Nalwa, 2004, p. 665.
14. J. L. Chen, Y. D. Li, Y. M. Ma et al., 'Formation of bamboo-shaped carbon filaments and dependence of their morphology on catalyst composition and reaction conditions', *Carbon*, 39, 1467 (2001).

15. N. Chandra, S. Namila, and C. Shet, Local elastic properties of carbon nanotubes in the presence of Stone-Wales defects, *Physical Review B* 69, 094101, (2004).
16. Chunyu Li and Tsu-Wei Chou, Axial and radial thermal expansions of single-walled carbon nanotubes, *Physical Review B* 71, 235414, (2005).
17. M.-F. Yu; et al. (2000). "Strength and Breaking Mechanism of Multiwalled Carbon Nanotubes Under Tensile Load". *Science*. 287 (5453): 637–40.
18. X. Zhang, T. Liu, T. V. Sreekumar, S. Kumar, V. Moore, R. Hauge, and R. E. Smalley, "Poly(vinyl alcohol)/SWNT Composite Film," *Nano Letters*, vol. 3, pp. 1285-1288, 2003.
19. R. S. Ruoff; et al. (1993). "Radial deformation of carbon nanotubes by van der Waals forces". *Nature*. 364 (6437): 514.
20. M. Minary-Jolandan, M.-F. Yu (2008). "Reversible radial deformation up to the complete flattening of carbon nanotubes in nanoindentation". *Journal of Applied Physics*. 103: 073516.
21. <http://www.jameshedberg.com/scienceGraphics.php?id=carbon-nanotube-FET>.
22. Biercuk, M.J.; et al., "Electrical transport in single-wall carbon nanotubes", *Topics in Applied Physics*; 111; 455-493. (2008).
23. Hong, Seunghun; Myung, S (2007). "Nanotube Electronics: A flexible approach to mobility". *Nature Nanotechnology*. 2 (4): 207–208.
24. W. D. J. Callister, *Materials Science and Engineering an Introduction*, 6th ed.:Wiley, 2003.
25. F. Li, M. Cheng, S. Bai, G. Su, and M. S. Dresselhaus, "Tensile strength of single-walled carbon nanotubes directly measured from their macroscopic ropes," *Applied Physics Letters*, vol. 77, pp. 3161-3164, 2000.
26. M.-F. Yu, O. Lourie, M. J. Dyer, K. Moloni, T. F. Kelly, and R. S. Ruoff, "Strength and Breaking Mechanism of Multiwalled Carbon Nanotubes Under Tensile Load," *Science*, vol. 287, pp. 637-640, 2000.
27. E. W. Wong, P. E. Sheehan, and C. M. Lieber, "Nanobeam Mechanics: Elasticity, Strength, and Toughness of Nanorods and Nanotubes," *Science*, vol. 277, pp. 1971-1975, 1997.
28. A. V. Melechko, V. I. Merkulov, T. E. McKnight, M. A. Guillorn, K. L. Klein, D. H. Lowndes, and M. L. Simpson, "Vertically aligned carbon nanofibers and

- related structures: Controlled synthesis and directed assembly," *Journal of Applied Physics*, vol. 97, pp. 041301-1-39, 2005.
29. P. Poncharal, C. Berge, Y. Yi, Z. L. Wang, and W. d. Heer, "Room temperature ballistic conduction in carbon nanotubes," *Journal of Physical Chemistry B*, vol. 106, pp. 12104-12118, 2002.
 30. A. Thess, R. Lee, P. Nikolaev, H. Dai, P. Petit, J. Robert, C. Xu, Y. H. Lee, S. G. Kim, A. G. Rinzler, D. T. Colbert, G.E.Scuseria, D. Tomanek, J. Fischer, and R. E. Smalley, "Crystalline Ropes of Metallic Carbon Nanotubes," *Science*, vol. 273, pp. 483-487, 1996.
 31. INTRODUCTION TO NANOSCALE SCIENCE AND TECHNOLOGY Edited by Massimiliano Di Ventra, Stephane Evoy, and James R. Heflin ISBN: 1-4020-7720-3
 32. S.Y. Chou, M.S. Wei, P.R. Krauss, P.B. Fisher, *J. Appl. Phys.* 76 (1994) 6673.
 33. C. Rao, R. Sen, B. Satishkumar, A. Govindaraj, *Chem. Commun.* 15 (1998) 1525.
 34. N. Grobert, W. Hsu, Y. Zhu, J. Hare, H. Kroto, D. Walton, M. Terrones, H. Terrones, Ph. Redlich, M. Rühle, R. Escudero, F. Morales, *Appl. Phys. Lett.* 75 (1999) 3363.
 35. A. Leonhardt, M. Ritschel, R. Kozhuharova, A. Graff, T. Mühl, R. Huhle, I. Mönch, D. Elefant, C.M. Schneider, *Diamond Related Mater.* 12 (2003) 790.
 36. T. Mühl, D. Elefant, A. Graff, R. Kozhuharova, A. Leonhardt, I. Mönch, M. Ritschel, P. Simon, S. Groudeva-Zotova, C.M. Schneider, *J. Appl. Phys.* 93 (10) (2003) 7894.
 37. N. Grobert, M. Mayne, M. Terrones, J. Sloan, R.E. Dunin-Borkowski, R. Kamalakaran, T. Seeger, H. Terrones, M. Rühle, D.R.M. Walton, H.W. Kroto, J.L. Hutchison, *Chem. Commun.* (2001) 471.
 38. J. Bao, C. Tie, Z. Xu, Z. Suo, Q. Zhou, J. Hong, *Adv. Mater.* 14 (2002) 1483.
 39. J. Nogues, V. Skumryev, J. Sort, S. Stoyanov and D. Givord, *Phys. Rev. Lett.*, 2006, 97, 157203.
 40. R. H. Baughman, A. A. Zakhidov and W. A. de Heer, *Science*, 2002, 297, 787; C. N. R. Rao and A. Govindaraj, *Nanotubes and Nanowires*, Royal Society of Chemistry, London, 2007.
 41. J. C. Lewenstein, T. P. Burgin, A. Ribayrol, L. A. Nagahara and R. K. Tsui, *Nano Lett.*, 2002, 2, 443.

42. B. Gao, Y. F. Chen, M. S. Fuhrer, D. C. Glattli and A. Bachtold, *Phys. Rev. Lett.*, 2005, 95, 196802.
43. S. Li, N. Liu, M. B. Chan-Park, Y. Yan and Q. Zhang, *Nanotechnology*, 2007, 18, 455302.
44. T. Brintlinger, M. S. Fuhrer, J. Melngailis, I. Utke, T. Bret, A. Perentes, P. Hoffmann, Abourida and P. Doppelt, *J. Vac. Sci. Technol., B*, 2005, 23, 3174.
45. J. O. Lee, C. Park, J. J. Kim, J. Kim, J. W. Park and K. H. Yoo, *J. Phys. D: Appl. Phys.*, 2000, 33, 1953.
46. Thiruvvelu Bhuvana, Kyle C. Smith, Timothy S. Fisher and Giridhar U. Kulkarni, Self-assembled CNT circuits with ohmic contacts using Pd hexadecanethiolate as in situ solder, *Nanoscale*, 2009, 1, 271–275.
47. Gu D, Li W, Wang F, Bongard H, Splithoff B, Schmidt W, Weidenthaler C, Xia Y, Zhao D, Schüth F, *Angew. Chem. Int. Ed.* 2015, 54, 7060-7064.
48. Nan Yan, Xuhui Zhou, Yan Li, Fang Wang, Hao Zhong, Hui Wang & Qianwang Chen, *Scientific Reports* 3, Article number: 3392 (2013).
49. Peihang Li, Mengnan Cui, Mingbo Zhang, Amin Guo, Yunfei Sun, Heng-guo Wang, Yanhui Li and Qian Duan, *CrystEngComm*, 2016, 18, 3383–3388.
50. Luis E. Hueso, Jose´ M. Pruneda, Valeria Ferrari, Gavin Burnell, Jose´ P. Valde´s-Herrera, Benjamin D. Simons, Peter B. Littlewood, Emilio Artacho, Albert Fert & Neil D. Mathur, *NATURE* | Vol 445 | 25 January 2007.
51. Jonker, B. T. & Flatte´, M. E. F. in *Nanomagnetism* (eds Mills, D. L. & Bland, J. A. C.) 227–272 (Elsevier, Amsterdam, 2006).
52. Datta, S. & Das, B. Electric analog of the electro-optic modulator. *Appl. Phys. Lett.* 56, 665–667 (1990).
53. <https://sites.ualberta.ca/~ccwj/teaching/microscopy/Figs/PNG/interactionvolume.png>
54. Hitachi Launches World’s Highest Resolution FE-SEM. *Nanotech Now*. 31 May 2011.
55. <http://publish.illinois.edu/x-raycrystallography/files/2014/12/Braggs-Law.jpg>
56. Catarina Costa Moura, Rahul S. Tare, Richard O. C. Oreffo, Sumeet Mahajan, Raman spectroscopy and coherent anti-Stokes Raman scattering imaging: prospective tools for monitoring skeletal cells and skeletal regeneration, *J. R. Soc. Interface* 13: 20160182, 2016.

57. Ran, Shannon K'doah (2004). Gravity Probe B: Exploring Einstein's Universe with Gyroscopes (PDF). NASA. p. 26.
58. S. Bedanta, O. Petracic, M. Aderholz, and W. Kleemann, A sample holder design for high temperature measurements in superconducting quantum interference device magnetometers, REVIEW OF SCIENTIFIC INSTRUMENTS 76, 0839102005.
59. R. Kozhuharova et al. / Applied Surface Science 238 (2004) 355–359.
60. Derbyshire, F.; Presland, A. E. B.; Trimm, D. L. Graphite formation by the dissolution-precipitation of carbon in cobalt, nickel and iron. Carbon 1975, 13, 111-113.
61. Baker, R. T. K.; Harris, P. S. In Chemistry and Physics of Carbon; Walker, P. L., Throver, P. A., Eds.; Marcel Dekker: New York, 1978; Vol. 14, p 83.
62. Baker, R. T. K. Catalytic Growth of Carbon Filaments. Carbon 1989, 27, 315-323.
63. Derbyshire, F.; Presland, A. E. B.; Trimm, D. L. Graphite formation by the dissolution-precipitation of carbon in cobalt, nickel and iron. Carbon 1975, 13, 111-113.
64. Liu et al. Chem. Mater., Vol. 12, No. 8, 2000.
65. Yang et al. , Appl. Phys. Lett., Vol. 82, No. 26, 30 June 2003.
66. Chiang et al. J. Phys. Chem. B, Vol. 105, No. 6, 2001.
67. Ajayan, P M et al. Nature; London 375.6532 (Jun 15, 1995): 564.
68. W. Y. Li, L. N. Xu, J. Chen, Adv. Funct. Mater., 2005.
69. Greenwood, Norman N.; Earnshaw, Alan (1997). Chemistry of the Elements (2nd). Butterworth-Heinemann. p. 1118.
70. Xiao-Ping Shen, Hua-Juan Miao, Hui Zhao, Zheng Xu, Synthesis, characterization and magnetic properties of Co₃O₄ nanotubes, Appl. Phys. A 91, 47–51 (2008).
71. V.G. Hadjiev, M.N. Iliev, I.V. Vergilov, J. Phys. C: Solid State Phys. 21, L199 (1988).
72. Greenwood, Norman N.; Earnshaw, Alan (1997). Chemistry of the Elements (2nd ed.). Butterworth-Heinemann. p. 1118. ISBN 0-08-037941-9.
73. Aakansha Kapoor, Nitesh Kumar Singh, A. K. Nigam, A. Bajpai, manuscript and preparation.

74. A. Bajpai, Z. Aslam, S. Hampel, R. Klingeler, N. Grobert, A carbon-nanotube based nano-furnace for in-situ restructuring of a magnetoelectric oxide, *Carbon* (2017), doi: 10.1016/j.carbon.2016.12.008.
75. R.V. Colvin, S. Arajs, Magnetic susceptibility of face-centered cubic cobalt just above the ferromagnetic Curie temperature, *Journal of Physics and Chemistry of Solids*, Volume 26, Issue 2, February 1965, Pages 435-437.
76. W. H. Meiklejohn and C. P. Bean, New Magnetic Anisotropy, *Phys. Rev.* 102, 5, 1413 (1956).
77. M. Terrones, N. Grobert, J. Olivares, J. P. Zhang, H. Terrones, K. Kordatos, W. K. Hsu, J. P. Hare, P. D. Townsend, K. Prassides, A. K. Cheetham, H. W. Kroto and D. R. M. Walton, *Nature* 388, 52-55 (1997).
78. Bajpai A, Gorantla S, Loeffler M, Hampel S, Ruemmeli MH, Thomas J, Ritschel, M, Gemming T, Büchner B, Klingeler R. The Filling of Carbon Nanotubes with Magnetoelectric Cr₂O₃, *Carbon*, 2011; 50: 1706.
79. A. Okamoto, H. Shinohara, Control of diameter distribution of single walled carbon nanotubes using the zeolite-ccvd method at atmospheric pressure, *Carbon* 43 (2) (2005) 431-436.
80. D. Srikala , V. N. Singh , A. Banerjee , B. R. Mehta , and S. Patnaik, Control of magnetism in cobalt nanoparticles by oxygen passivation, *J. Phys. Chem. C* 112, 13882 (2008).
81. R. V. Colvin and S. Arajs, Magnetic susceptibility of face-centered cubic cobalt just above the ferromagnetic Curie temperature, *J. Phys. Chem. Solids* , Vol. 26, pp. 435-437 (1965).
82. W. H. Meiklejohn and C. P. Bean, New magnetic anisotropy, *Physical review*, vol -105, number 3 (1957).
83. Prof. Dr. Guoxiu Wang, Hao Liu, Prof. Josip Horvat, Bei Wang, Prof. Dr. Shizhang Qiao, Jinsoo Park, Prof. Dr. Hyojun Ahn, Highly Ordered Mesoporous Cobalt Oxide Nanostructures: Synthesis, Characterisation, Magnetic Properties, and Applications for Electrochemical Energy Devices, *Chem. Eur. J.* 2010, 16, 11020 – 11027.
84. S.-L. Chou et al., Electrochemical deposition of porous Co₃O₄ nanostructured thin film for lithium-ion battery/ *Journal of Power Sources* 182 (2008) 359–36.